Genesis of hyper-enriched black shale Ni-Mo-Zn-Pt-Pd-Re mineralization in the northern Canadian Cordillera

M.G. Gadd[1*], J.M. Peter[1], and D. Layton-Matthews[2]

Gadd, M.G., Peter, J.M., and Layton-Matthews, D., 2022. Genesis of hyper-enriched black shale Ni-Mo-Zn-Pt-Pd-Re mineralization in the northern Canadian Cordillera; in *Targeted Geoscience Initiative 5: volcanic- and sediment-hosted massive-sulfide deposit genesis and exploration methods, (ed.) J.M. Peter and M.G. Gadd; Geological Survey of Canada, Bulletin 617, p. 15–38. https://doi.org/10.4095/328013*

Abstract: Polymetallic (Ni-Mo-Zn-Pt-Pd-Au-Re) hyper-enriched black shales in the northern Canadian Cordillera consist of thin, semi-massive sulfides interbedded with black shale. We studied HEBS deposits at Nick, Peel River, Monster River, and Moss in northern Yukon, and at a single locality underlying the Cardiac Creek Pb-Zn-Ag deposit in northeastern British Columbia. High-grade mineralization contains up to 7.4 weight per cent Ni, 2.7 weight per cent Zn, 0.38 weight per cent Mo, 400 ppb Pt, 250 ppb Pd, 160 ppb Au, and 58.5 ppm Re. Sulfide mineralization formed during syngenesis to later diagenesis. Analyses by LA-ICP-MS indicate that pyrite is the principal host of platinum-group elements, Au, and Re. Mineralization and sedimentation were coeval based on the overlap between Re-Os geochronology of HEBS at Nick and Peel River (390.7 ± 5.1 and 387.3 ± 4.4 Ma, respectively) and conodont biostratigraphic ages of sedimentary host rocks. Bulk S isotope composition of HEBS is uniformly negative, indicating that bacterial reduction of seawater sulfate generated sulfur to precipitate sulfide minerals. The initial Os ratios at Peel River (0.25 ± 0.07) and Nick (0.32 ± 0.20) overlap with Middle Devonian seawater, suggesting that elemental enrichment was derived from seawater.

Résumé : Dans le nord de la Cordillère canadienne, des shales noirs surenrichis renferment une minéralisation polymétallique (Ni-Mo-Zn-Pt-Pd-Au-Re) constituée de fines couches de sulfures semi-massifs interstratifiées dans les shales. Nous avons étudié cette minéralisation de shales noirs surenrichis aux gîtes de Nick, de Peel River, de Monster River et de Moss, dans le nord du Yukon, ainsi qu'à un endroit isolé où une telle minéralisation est présente sous le gisement de Pb-Zn-Ag de Cardiac Creek, dans le nord-est de la Colombie-Britannique. La minéralisation à forte teneur contient jusqu'à 7,4 % en poids de Ni, 2,7 % en poids de Zn, 0,38 % en poids de Mo, 400 ppb de Pt, 250 ppb de Pd, 160 ppb de Au et 58,5 ppm de Re. La minéralisation sulfurée est de formation syngénétique à tardigénétique. Les analyses par LA-ICP-MS (spectrométrie de masse avec plasma à couplage inductif jumelée à l'ablation par laser) révèlent que la pyrite est la principale phase hôte des éléments du groupe du platine, de Au et de Re. La minéralisation est contemporaine de la sédimentation d'après le chevauchement de la géochronologie Re-Os des shales noirs surenrichis des gîtes de Nick et de Peel River (390,7 ± 5,1 et 387,3 ± 4,4 Ma, respectivement) et des âges biostratigraphiques révélés par des conodontes présents dans les roches hôtes sédimentaires. La composition isotopique du soufre dans des échantillons en vrac de shales noirs surenrichis est uniformément négative, ce qui indique qu'une réduction bactérienne des sulfates de l'eau de mer a produit le soufre qui a précipité sous forme de minéraux sulfurés. Les rapports initiaux de Os aux gîtes de Peel River (0,25 ± 0,07) et de Nick (0,32 ± 0,20) chevauchent ceux de l'eau de mer du Dévonien moyen, ce qui suggère que l'enrichissement en Os tire sa source de l'eau de mer.

[1]Geological Survey of Canada, 601 Booth Street, Ottawa, Ontario K1A 0E8
[2]Queen's Facility for Isotope Research, Department of Geological Sciences and Geological Engineering at Queen's University, 36 Union Street, Kingston, Ontario K7L 3N6
*Corresponding author: M.G. Gadd (email: michael.gadd@nrcan-rncan.gc.ca)

INTRODUCTION AND BACKGROUND INFORMATION

Hyper-enriched black shale (HEBS), also referred to as highly metalliferous black shale (Johnson et al., 2017), is an important global repository for Zn, Ni, Cu, Mo, Se, U, V, Cr, Co, Ag, Au, Re, platinum-group elements (PGE), and rare-earth elements (REE; Jowitt and Keays, 2011). Johnson et al. (2017) defined HEBS as having Mo+Ni+Zn+Se+V greater than 1500 ppm, which is more than three times higher than the United States Geological Survey black shale standard SDO-1 (Kane, 1993). The best known example of HEBS in Canada is the Nick Ni-Zn-Mo-PGE-Re-Au prospect, Yukon (Hulbert et al., 1992), which was discovered in 1981 by Cominco while following up on a Geological Survey of Canada stream-sediment survey (Garrett et al., 1977; Parry and Carne, 1989). The nickel sulfide layer at the Nick prospect is thin (3–10 cm) and discontinuously crops out over a strike length of 100 km (Parry and Carne, 1989). This style of mineralization has been recognized in many locations across northern Yukon, including at Peel River (Dumala, 2007b, c; Crawford et al., 2019), Moss (Dumala, 2007d; Gadd et al., 2019a) and Rein (Caulfield, 1997; Fig. 1). Hyper-enriched black shale mineralization was thought to be absent at Monster River (Dumala, 2007b); however, HEBS with a composition typical of other Yukon examples was identified there during summer 2018 (Gadd, Peter, Fraser et al., this volume). At least four other localities with a HEBS metal enrichment signature (Ni, Mo, Zn anomalies) in surficial media have been identified, but bedrock mineralization has not yet been located (Gregory, 2008a, b, c, d). Polymetallic HEBS have also been recently discovered in the Kechika trough, which is the southern extension of the Selwyn Basin in northeastern British Columbia (Fig. 1; Peter et al., 2018a). The HEBS mineralization that underlies the Cardiac Creek sedimentary exhalative (SEDEX) Ag-Pb-Zn-Ba deposit in British Columbia (Peter et al., 2018a) is mineralogically and geochemically similar to that in Yukon. This HEBS is interpreted to be the same age as those in Yukon (Gadd et al., 2020) but is more than 1000 km away from the nearest exposure in Yukon.

Hyper-enriched black shale deposits in Yukon and British Columbia (Fig. 1) are well endowed with metals and contain up to 7.4 weight per cent Ni, 2.7 weight per cent Zn, 0.38 weight per cent Mo, 400 ppb Pt, 250 ppb Pd, 160 ppb Au, and 58.5 ppm Re (Table 1). Despite exceptional metal grades and intensive exploration, the HEBS in northwestern Canada has not been studied in detail and their genesis is poorly understood. There is significant potential for further discoveries, but the lack of understanding of HEBS genesis hampers exploration. To address this, we conducted a five-year research program that applied multiple investigative methods to determine the origin and nature of these metal-rich shale deposits across the Canadian Cordillera in Yukon and British Columbia. Several concurrent research avenues were pursued. This work involved lithogeochemical studies (Gadd and Peter, 2018; Crawford et al., 2019; Gadd et al. 2019a; Gadd, Peter, Fraser et al., this volume), stable (i.e. S, Mo, and Tl) and radiogenic (i.e. Re-Os) isotopic studies (Crawford et al., 2019; Gadd et al., 2019a, 2020; Gadd et al., work in progress, 2021), and mineralogical studies (Gadd and Peter, 2018; Peter et al., 2018a; Gadd et al., 2019b). In this paper, we summarize the salient findings on the formation of HEBS using the examples we studied in northern Yukon and British Columbia. We also present exploration guidelines and implications resulting from these findings.

REGIONAL GEOLOGY

Richardson and Blackstone troughs

Hyper-enriched black shale mineralization in northern Yukon is located within Paleozoic basinal strata of the Richardson and Blackstone troughs (Fig. 1). The Richardson trough is bounded to the east by the Mackenzie platform and to the west by the Yukon block (Fig. 1), which were stable shelf features during the early Paleozoic (Morrow, 1999). The Blackstone trough is on the south margin of the Yukon block and is stratigraphically continuous with the Richardson trough (Norris, 1997). Sedimentary strata within the Richardson and Blackstone troughs are characterized by less than 1000 m of fine-grained, carbonaceous siliciclastic rocks of the upper Cambrian to Middle Devonian Road River Group (Fig. 1, 2a; Norris, 1997; Morrow, 1999; Strauss et al., 2020). The Canol Formation overlies the Road River Group and consists of up to approximately 220 m of Middle Devonian to early Upper Devonian cherty, carbonaceous shale (Fraser and Hutchison, 2017). The Late Devonian Imperial Formation, a deep-water shale interbedded with turbiditic sandstone, overlies the Canol Formation (Lane, 2007).

Hyper-enriched black shale mineralization is at the stratigraphic contact between the Road River Group and Canol Formation (Fig. 2b–e, 3a, b). The HEBS layer is thin (1–10 cm) and consists of approximately 40 to 60 volume per cent sulfides interbedded with black, siliceous shale (Fig. 3c, d; Hulbert et al., 1992; Gadd et al., 2019b). The upper and lower contacts with the enclosing host rocks are typically sharp, but minor slumping into the underlying siliceous shales may be locally present (Fig. 3d). There is minor to abundant biogenic debris present that includes conodont elements and pyrite permineralized plant matter (Fig. 3c; Gadd and Peter, 2018) and a relatively low abundance of terrigenous clastic detritus (Table 1; Gadd et al., 2019a). Igneous rocks are not present within the vicinity of any of the HEBS localities, but Upper Devonian plutonic rocks occur northeast of the Richardson trough (>100 km from nearest HEBS; Lane, 2007).

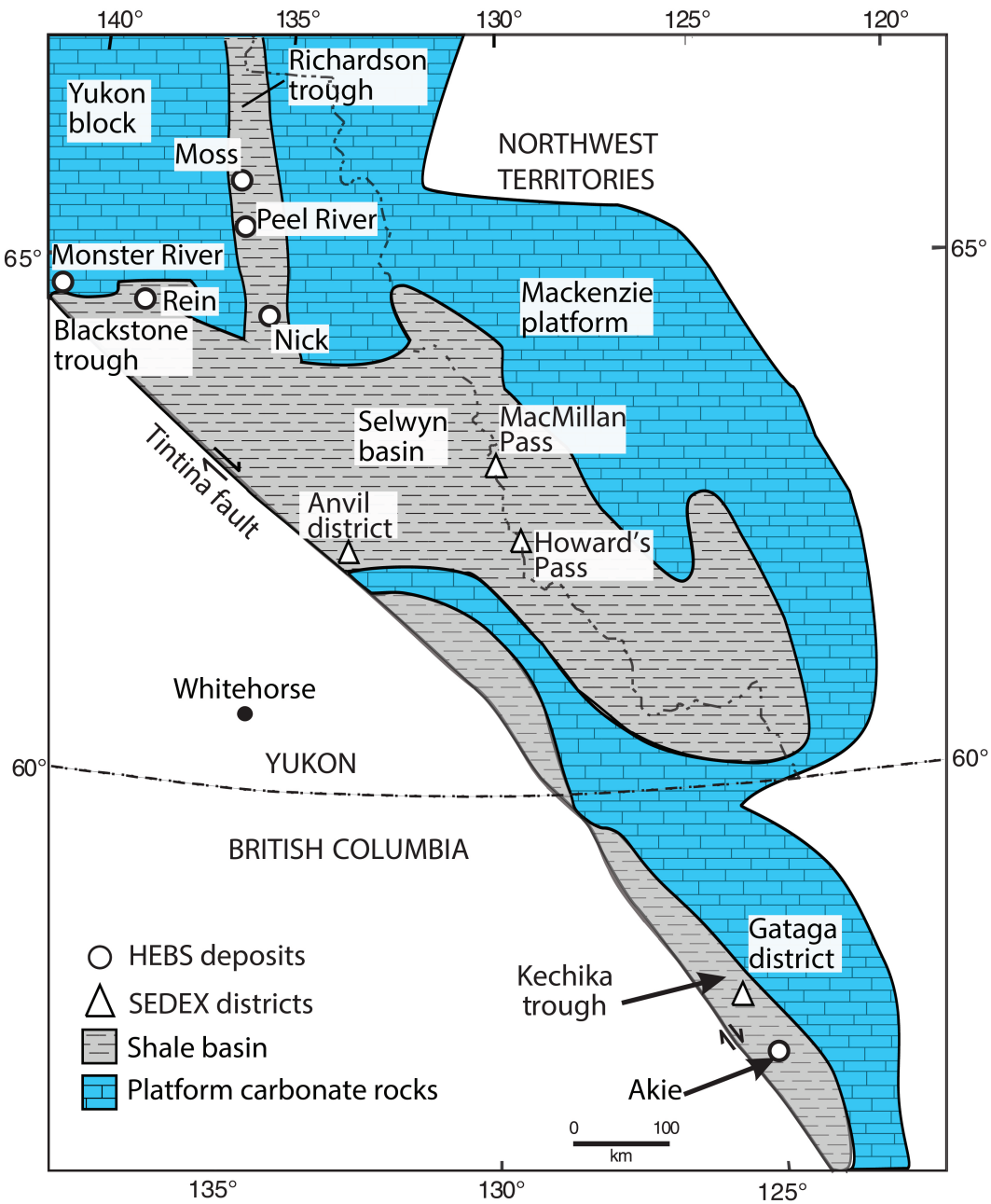

Figure 1. Map of the ancestral North American passive continental margin displaying locations of key hyper-enriched black shale (HEBS) localities and sedimentary exhalative (SEDEX) Zn-Pb districts (*modified from* Goodfellow, 2007) in British Columbia, Yukon, and Northwest Territories.

The nature of the contact between the Road River Group and the overlying Canol Formation has been variably interpreted as conformable, disconformable, and unconformable (e.g. Pugh, 1983; Morrow, 1999; Fraser and Hutchison, 2017). Recent research indicates that the contact is likely conformable and the uppermost portion of the Road River Group is a condensed section (Fraser and Hutchison, 2017; Gadd and Peter, 2018; Gadd et al., 2020). Condensed sections form in response to shoreline transgressions and are generally considered to represent maximum flooding surfaces (Loutit et al., 1988) that are starved of clastic sediments, so that thin (centimetre-scale) beds represent relatively long durations of sedimentation (Schutter, 1996). Several criteria are used to identify condensed sections (Schutter, 1996); criteria relevant to the HEBS in Yukon are high abundances of authigenic minerals (e.g. carbonate concretions outlined in Fig. 3a, b), abundant biogenic debris (e.g. petrified wood in Fig. 3c), and high abundances of metals and widespread geographic distribution (Fig. 4a–d).

Contents

Table 1. Range and mean abundance values of major, minor, and trace elements in hyper-enriched black shale (HEBS) and surrounding strata from localities in Yukon and British Columbia.

Element	Unit	Nick HEBS		Peel River N HEBS		Peel River S HEBS		Moss HEBS		Monster River HEBS		Akie HEBS		Road River Group		Canol Formation	
		Range (n = 11)	Mean	Range (n = 6)	Mean	Range (n = 16)	Mean	Range (n = 4)	Mean	Range (n = 5)	Mean	Range (n = 7)	Mean	Range (n = 171)	mean	Range (n = 55)	mean
Na_2O	wt %	0.06–0.19	0.11	0.05–0.08	0.07	0.03–0.06	0.04	0.02–0.03	0.02	0.13–0.20	0.17	0.03–0.23	0.09	0.01–0.71	0.19	0.03–1.18	0.14
MgO	wt %	0.19–0.46	0.31	0.05–2.08	0.47	0.03–0.14	0.07	0.03–0.10	0.05	0.30–0.36	0.33	0.46–5.62	2.02	0.07–17.34	1.76	0.06–4.36	0.39
SiO_2	wt %	37.30–73.60	49.07	35.37–73.6	43.36	23.88–40.81	31.58	23.29–31.78	26.65	33.8–40.8	38.87	1.7–56.8	33.19	2.6–98.3	59.24	21.72–96.6	85.35
Al_2O_3	wt %	2.15–5.75	3.67	1.47–4.32	3.03	0.63–2.96	1.77	0.87–1.70	1.16	4.36–5.90	5.09	0.44–14.9	7.44	0.56–17	6.87	1–8.41	3.22
P_2O_5	wt %	0.03–0.31	0.12	0.12–0.97	0.48	0.04–1.12	0.36	0.01–0.06	0.03	1.02–3.98	2.45	0.38–5.9	2.01	0.01–1.87	0.18	0.01–0.22	0.05
K_2O	wt %	0.51–1.44	0.91	0.36–1.12	0.79	0.16–0.86	0.53	0.08–0.34	0.16	1.01–1.63	1.35	0.11–5.78	2.7	0.06–5.29	1.90	0.11–1.96	0.74
CaO	wt %	0.06–0.37	0.16	0.62–5.66	1.77	0.08–1.51	0.56	0.06–0.22	0.15	1.56–5.49	3.5	1.31–53.7	20.02	0.01–54.38	10.08	0.01–39.91	1.95
TiO_2	wt %	0.09–0.31	0.18	0.08–0.15	0.11	0.02–0.11	0.02	0.03–0.07	0.04	0.21–0.50	0.29	0.02–0.48	0.26	0.03–1.77	0.44	0.04–0.42	0.15
MnO	wt %	0.01–0.02	0.01	0.01–0.02	0.02	0.01–0.02	0.01	0.02–0.03	0.02	0.01	0.01	0.01–0.1	0.03	0–0.09	0.02	0–0.05	0.01
$Fe_2O_{3(Total)}$	wt %	5.64–28.8	19.73	14.35–29.88	24.51	24.21–38.84	31.2	34.07–39.54	36.85	14.10–16.00	15.14	0.45–9.65	5.36	0.07–8.42	2.48	0.1–6.69	1.28
SrO	wt %	0.01-0.01	0.01	0.005-0.02	0.01	0.003-0.043	0.02	0.002-0.004	0.003	0.02-0.03	0.03	0.04-0.09	0.068	0.003–0.236	0.03	0.002–0.111	0.01
BaO	wt %	0.22-0.51	0.4	0.17-0.5	0.3	0.23-1.99	0.7	0.04-0.12	0.1	0.34-0.48	0.4	0.02-0.52	0.3	0.04–37.83	0.92	0.08–2.61	0.32
TIP (Al+Ti+K+Na)	wt %	2.82–7.67	4.86	1.97–5.67	4	0.84–3.98	2.41	1.03–2.14	1.39	5.71–8.12	6.9	0.6–21.37	10.5	0.71–23.86	9.40	1.28–11.1	4.25
C_{org}	wt %	2.01–3.94	3.01	1.16–1.51	1.36	1.12–2.28	1.61	1.47–1.78	1.65	3.98–5.57	5.1	0.34–5.24	4.02	0.56–8.74	2.57	1.03–5.93	2.56
CO_2	wt %	–	–	0.44–8.61	2.1	0.31–1.60	0.81	0.51–0.99	0.72	–	–	0.4–38.1	14.5	0.03–42.5	9.39	0.02–28.3	2.48
C_{total}	wt %	2.12–4.07	3.14	1.49–3.82	1.94	1.05–2.42	1.78	1.65–1.98	1.86	4.08–5.96	5.28	4.11–12.9	8.37	0.67–14.9	4.78	1.12–9.5	2.98
S_{total}	wt %	5.86–28.30	20.99	15.90–30.00	24.42	26.80–37.90	32.33	34.30–39.50	37.5	14.90–17.35	15.64	0.46–6.92	4.18	0.08–11.7	1.88	0.11–5.65	1.06
$S_{sulfide}$	wt %	5.32–26.4	19.34	14.60–19.10	16.85	–	–	–	–	10.00–14.55	12.38	0.31–7.34	3.76	0.04–5.28	1.54	0.07–5.78	0.98
Sc	ppm	2.2–6.1	3.8	2019–02–05	3.7	1.0–6.0	2.5	1.0–2.0	1.3	5.5–9.3	7	0.8–15.3	8.5	0.5–20.2	7.54	1–10	3.95
V	ppm	628–1700	1027.3	121–796	378.5	118–269	167.2	188–304	222.8	539–953	753.5	37–603	342	80–2310	903.51	56–1410	455.82
Cr	ppm	40–120	74.6	80–110	103.3	20–160	74	40–70	55	80–120	105	10–360	106	20–330	81.69	20–270	74.81
Co	ppm	12.7–153	107	57.4–186	119.6	50.4–209	140.6	111–149	130	199–536	373	7–70.5	33.3	0.5–30	7.82	0.3–14.9	3.13
Ni	ppm	11 600–39 100	28 636	11 800–49 000	30 950	29 100–73 900	42 660	31 100–41 000	35 425	16 500–53 900	34 900	622–31 100	6164	9.2–956	198.65	8.9–391	80.17
Cu	ppm	64.6–338	227	94.5–493	286	103–257	169	163–211	185	306–449	381	31.3–378.0	138.5	3.5–184	38.67	1.7–84	21.92

Table 1 (cont.). Range and mean abundance values of major, minor, and trace elements in hyper-enriched black shale (HEBS) and surrounding strata from localities in Yukon and British Columbia.

Element	Unit	Nick HEBS		Peel River N HEBS		Peel River S HEBS		Moss HEBS		Monster River HEBS		Akie HEBS		Road River Group		Canol Formation	
		Range (n = 11)	Mean	Range (n = 6)	Mean	Range (n = 16)	Mean	Range (n = 4)	Mean	Range (n = 5)	Mean	Range (n = 7)	Mean	Range (n = 171)	mean	Range (n = 55)	mean
Zn	ppm	144–8030	3175	938–27200	7360	239–23900	7458	451–1720	842	1580–4780	2300	541–12800	4557	16–3850	594.66	4–854	132.85
Ga	ppm	6.6–15.2	11.2	3.5–26.2	9.8	2.5–17	7.9	2.9–5.7	3.7	9.8–11.6	10.6	1.1–17.3	10.4	0.2–27.4	10.59	1.5–11.5	4.83
Ge	ppm	–	–	2.3–11.9	4.4	6.1–21.9	9.8	10.6–13.5	12	–	–	–	–	0.1–0.9	0.29	0.1–0.1	0.10
As	ppm	680–2860	1965	961–3080	2314	2660–5140	4204	4240–5500	4740	2180–2730	2462	26.9–420	243	2.6–143	27.99	1.7–108.5	16.12
Se	ppm	600–1100	855	497–2570	1050	1320–4450	2073	1760–2450	2135	1300–3200	2250	27.9–800	178	1.1–277	19.62	0.4–65.2	11.79
Rb	ppm	20.2–54.9	35.17	14–37	28.5	4.0–33	18.4	7.0–18.0	9.8	33.6–44.3	39	3.3–134.5	69.9	3–207	67.79	4–78	29.36
Zr	ppm	29–79	53.4	19–44	29.5	9.0–25	15.3	12.0–22	15.5	63–100	83	13–127	77	9–337	89.81	13–70	29.24
Nb	ppm	2.1–7.3	4.1	1.3–3.1	1.9	0.2–2.0	1	0.5–1.3	0.8	7.9–20.7	11.1	0.6–11.8	5.7	0.3–61.7	11.37	0.8–6	2.50
Mo	ppm	1185–3830	1969	554–3170	1976	1530–3310	2573	2370–2980	2733	650–764	719	27–203	96	3.13–177	39.00	5.1–120.5	37.26
Ag	ppm	4.51–8.37	6.69	0.69–6.86	2.83	1.42–2.08	1.73	2.07–2.25	2.16	3.7–6.29	5.14	0.42–3.94	1.59	0.07–3.75	0.72	0.06–1.98	0.39
Cd	ppm	1.1–61.2	24.6	4.1–74.7	26.9	0.5–108	33.4	2.1–6.6	3.8	15.5–34.1	22.5	3.52–57.3	19	0.06–103	8.89	0.04–10.4	1.43
In	ppm	0.02–0.45	0.23	0.1–0.2	0.15	0.1–0.7	0.25	–	–	0.04–0.08	0.06	0.02–0.05	0.03	0–0.12	0.04	0.01–0.02	0.02
Sn	ppm	2–4	3	1–7	3	2–12	6	1	1	1	1	1	1	1–3	2	1–2	1
Sb	ppm	22.2–82.6	52.2	40.1–155	79.3	68.2–193	135	109–129	117.3	146–202	175	3.7–67.2	33.7	0.42–23.8	7.37	0.2–13.9	4.29
Te	ppm	1.1–2.31	1.8	3.1–31	8.8	1–2.1	1.5	18.5–21.3	19.8	11.7–46.2	28.3	0.18–2.0	0.6	0.02–1.5	0.35	0.03–1.1	0.35
Cs	ppm	0.71–1.98	1.2	0.8–2.0	1.38	0.2–1.6	0.91	0.3–1.0	0.5	1.80–2.17	1.96	0.17–7.97	3.72	0.1–14.2	3.84	0.2–4.2	1.52
La	ppm	14.5–153.5	75.7	22.9–55.1	39	2.03–180	37.8	2.91–7.01	4.61	43.4–107.5	83.2	24–82.8	42.6	2.4–101	27.37	2.94–43.2	10.11
Ce	ppm	17.2–139	73.7	32.7–69.3	52.5	3.01–232	51.1	5.35–12.5	8.5	51.6–135.5	100.5	26–75.8	57.2	2.4–172.5	39.69	4.63–57.4	15.64
Pr	ppm	3.68–34.5	17.74	5.56–13.4	9.83	0.5–36.7	9.27	1.04–2.55	1.84	12.1–25.9	20	3.79–15.85	9.38	0.45–25.7	5.90	0.73–8.98	2.41
Nd	ppm	15.7–142.5	74.9	20.7–54.6	39.1	2.53–102	36.6	5.13–13.6	9.6	51.7–102.0	80.9	13.7–67.5	39.4	1.52–109.5	22.99	3.17–48	9.70
Sm	ppm	3.32–26.3	13.3	3.06–10.9	7.24	0.8–28.1	8.07	0.96–3.578	1.92	10.65–18.75	15.29	2.09–12.7	7.8	0.28–22.2	4.32	0.54–15.1	1.99
Eu	ppm	0.57–4.70	2.45	0.63–2.37	1.51	0.17–6.3	1.82	0.17–0.72	0.33	2.15–4.71	3.7	0.42–3.12	1.71	0.08–5.46	0.96	0.04–3.93	0.45
Gd	ppm	3.17–26.5	13.8	2.29–9.78	6.54	0.59–28.5	7.32	0.68–3.27	1.52	10.55–20.90	17.06	2.1–14.75	8.23	0.33–22	4.18	0.26–18.7	2.02
Tb	ppm	0.44–3.56	1.88	0.36–1.51	1.02	0.08–4.16	1.03	0.1–0.45	0.22	1.41–2.89	2.34	0.28–2.05	1.13	0.03–3.15	0.63	0.03–3.12	0.33
Dy	ppm	3.2–23.8	12.32	1.93–8.59	5.79	0.35–22.6	5.69	0.57–2.28	1.16	8.27–16.35	13.53	1.75–12.8	6.91	0.3–17.9	3.77	0.32–17.8	2.02
Y	ppm	25.9–219	112.5	13.7–77.6	50.3	2.4–193	47.8	3.4–12.3	6.7	57–154.5	117.2	25.5–137.5	61.7	2.1–189	28.82	2.2–169	17.09

Contents

Table 1 (cont.). Range and mean abundance values of major, minor, and trace elements in hyper-enriched black shale (HEBS) and surrounding strata from localities in Yukon and British Columbia.

Element	Unit	Nick HEBS		Peel River N HEBS		Peel River S HEBS		Moss HEBS		Monster River HEBS		Akie HEBS		Road River Group		Canol Formation	
		Range (n = 11)	Mean	Range (n = 6)	Mean	Range (n = 16)	Mean	Range (n = 4)	Mean	Range (n = 5)	Mean	Range (n = 7)	Mean	Range (n = 171)	mean	Range (n = 55)	mean
Ho	ppm	0.66–5.02	2.6	0.36–1.78	1.18	0.06–4.45	1.12	0.11–0.38	0.21	1.50–3.31	2.69	0.41–2.64	1.37	0.06–3.49	0.77	0.07–3.63	0.43
Er	ppm	1.92–15.7	7.98	1.01–5.04	3.21	0.16–11.7	2.96	0.29–1.02	0.55	4.39–9.19	7.56	1.26–7.61	3.86	0.2–10.6	2.29	0.24–9.71	1.26
Tm	ppm	0.25–1.89	1	0.13–0.65	0.4	0.02–1.43	0.36	0.04–0.13	0.07	0.56–1.16	0.9	0.18–0.91	0.5	0.03–1.44	0.32	0.02–1.24	0.18
Yb	ppm	1.33–11.65	6.2	0.74–3.74	2.36	0.14–7.91	2.02	0.26–0.77	0.43	3.25–6.55	5.24	1.21–5.07	2.98	0.22–8.51	2.10	0.24–7.83	1.17
Lu	ppm	0.2–1.61	0.88	0.11–0.53	0.33	0.02–1.11	0.28	0.04–0.10	0.06	0.45–0.94	0.72	0.17–0.71	0.41	0.03–1.31	0.32	0.03–1.21	0.18
∑REE–Y	ppm	92.2–808.9	417	106.2–307.5	220.3	12.9–636.9	213.2	21.9–60.7	37.6	260.5–595.2	470.8	102.9–427.9	245.2	10.62–619.54	144.43	17.71–373.95	64.99
Ce-Ce*	—	0.44–0.54	0.48	0.59–0.67	0.62	0.54–0.70	0.64	0.63–0.71	0.67	0.52–0.62	0.56	0.39–0.86	0.69	0.41–0.85	0.69	0.55–0.94	0.72
Pr-Pr*	—	1.26–1.39	1.34	1.21–1.25	1.23	1.03–1.39	1.19	1.11–1.22	1.17	1.23–1.35	1.28	1.02–1.39	1.12	1–1.33	1.14	0.96–1.3	1.14
Eu-Eu*	—	0.8–0.88	0.84	0.94–1.11	1.03	0.97–1.29	1.09	0.77–0.98	0.9	0.91–1.14	1.05	0.84–1.12	0.98	0.26–4.46	1.05	0.5–1.38	0.98
Y-Ho	—	37.5–45.7	42	37.2–46.5	41.3	34.7–51.7	41.2	30.9–34.2	32.5	36.3–47.0	42.5	35.4–62.2	46.1	27.16–54.15	38.36	26.67–59.3	35.46
Hf	ppm	0.6–2.0	1.14	0.5–1.1	0.7	0.1–0.7	0.3	0.2–0.3	0.22	1.3–1.8	1.65	0.3–3.6	2.1	0.1–8.3	2.14	0.3–1.7	0.69
Ta	ppm	0.1–0.5	0.3	0.1–0.5	0.2	0.03–0.15	0.07	0.05–0.11	0.07	0.4–0.7	0.6	0.2–0.9	0.5	0.02–3.7	0.74	0.05–0.61	0.21
W	ppm	3.0–13	6	1.4–6.2	3.2	1.0–4.1	2.7	2.1–3.7	3	1	1	1	1	0.5–11.7	1.84	0.5–3.4	1.43
Re	ppm	13.15–25.5	19.46	7.55–32.0	14.69	24.5–55.0	35.48	33.5–58.5	44.9	12.4–32.7	22.6	0.242–8.12	1.74	0.002–0.433	0.06	0.003–0.65	0.07
Hg	ppm	0.647–1.54	1.08	0.8–3.46	1.87	0.96–2.17	1.36	2.06–2.41	2.31	2.23–4.95	3.62	0.27–2.38	0.81	0.01–0.6	0.13	0.02–0.33	0.10
Tl	ppm	57.3–195	134.6	107–434	214.3	202–500	350.9	278–402	341	41.6–84.9	60.77	1.83–11.2	5.1	0.12–34.2	3.75	0.11–13.6	2.35
Pb	ppm	41.9–118	90.3	17.4–64.2	37.3	7.6–27.6	14.6	37.8–52.7	44.5	42.8–76.7	59	46.5–6740	1163	0.6–22.3	9.09	1.3–12.1	5.27
Bi	ppm	0.46–1.48	1.07	0.31–1.03	0.57	0.37–1.12	0.64	0.53–0.67	0.61	0.91–1.66	1.26	0.04–0.83	0.34	0.01–0.37	0.12	0.02–0.25	0.09
Th	ppm	1.73–5.01	3.07	1.58–11.7	4.7	0.36–2.8	1.41	0.56–1.1	0.76	2.83–3.60	3.26	1.02–11.1	6	0.3–11.55	4.51	0.64–5.8	1.91
U	ppm	5.19–67.6	39.1	9.65–49.4	30.1	2.85–79.4	25.8	2.6–5.98	4.1	60.9–92.0	79.8	9.51–71.3	39.7	0.64–46.5	10.46	1.14–14.8	5.07
Ir	ppb	1–5	2	0.5–1.6	1.0	0.5–2.8	1.2	0.8–1.3	1.0	2–4	3	1.0–2	1.5	0.1–3	0.65	0.1–2	0.75
Ru	ppb	3–19	8	<5	<5	<5–61	19.3	6–9	8	6–17	10.7	4.0–27	16.25	3–31	7.93	3–7	3.90
Rh	ppb	2–3	2	1.0–4.5	2.6	1.9–5.8	2.9	2.9–3.5	3.2	2–6	2.8	2	2	0.2–4	0.48	0.2–2	0.39
Pt	ppb	92–276	191	64–239	151.8	189–413	243.6	255–368	302.5	240–342	286	4–113	30.17	2–18	4.63	2–14	6.25
Pd	ppb	49–120	94	45–150	100.5	114–255	149.4	154–228	188.5	105–183	143	3–57	16.83	2–33	4.47	2–17	3.97
Au	ppb	17–54	31	39.7–100	74.3	57.2–129	93.6	121–167	144.8	42–56	52	10–57	26.25	0.5–149	5.63	0.5–52	3.64

Note: Ce-Ce* = $Ce_N/(La_N \times Pr_N)^{0.5}$; Eu-Eu* = $Eu_N/(Sm_N \times Gd_N)^{0.5}$; Pr-Pr* = $Pr_N/(Ce_N \times Nd_N)^{0.5}$
N: normalized to Post–Archean Australian Shale (McLennan, 1989); TIP: Terrestrial input

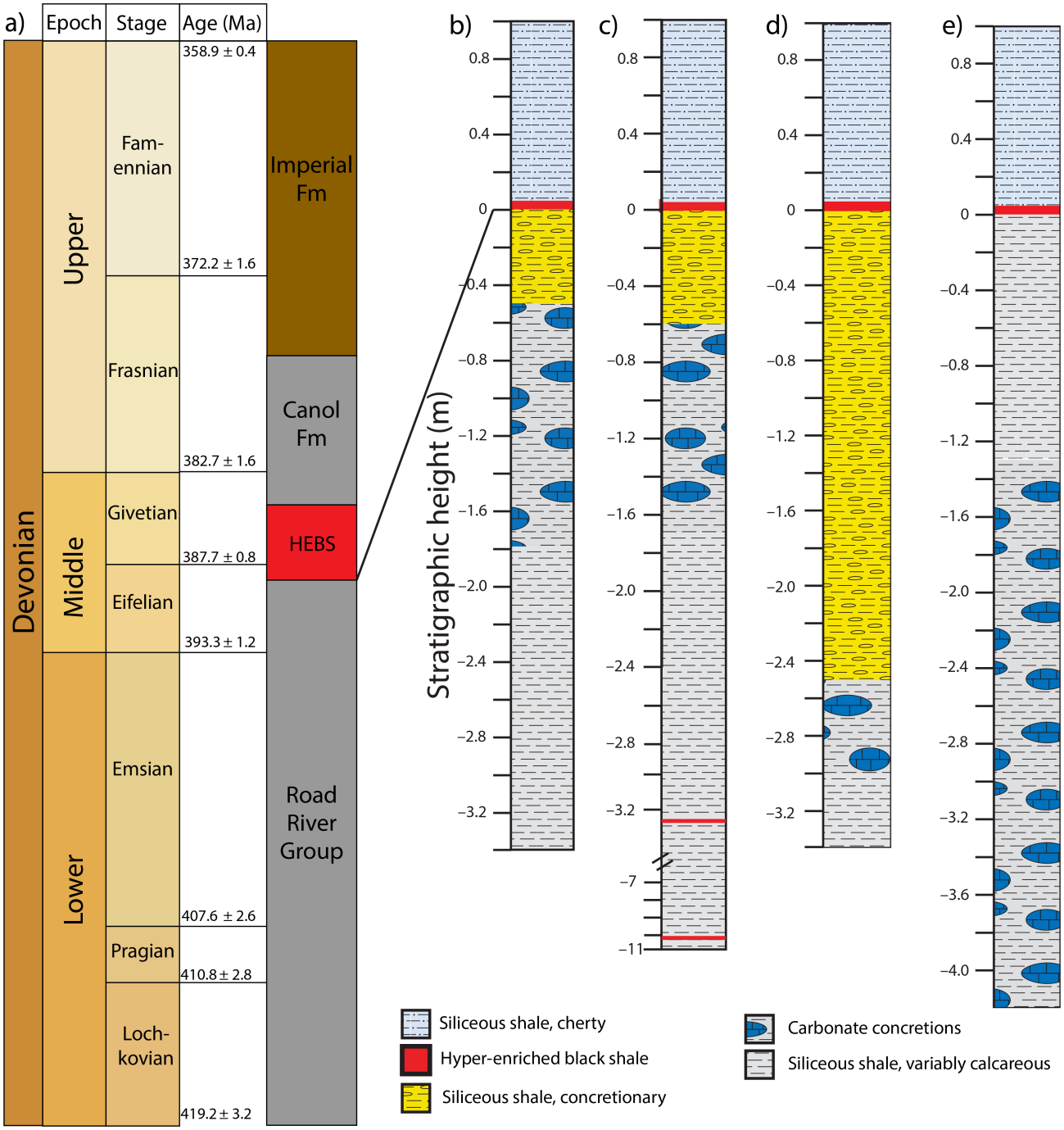

Figure 2. a) Devonian stratigraphy of Richardson trough in northern Yukon with schematic stratigraphic sections that highlight the lithostratigraphy at the **b)** Eagle Plains, **c)** Peel River (note break in scale below –3.2 m), **d)** Monster River, and e) Nick hyper-enriched black shale (HEBS) localities. The 0 m mark is positioned at the base of the HEBS layer, which occurs at the stratigraphic contact between the Road River Group and the Canol Formation. The ages are based on the Devonian time scale of Becker et al. (2012).

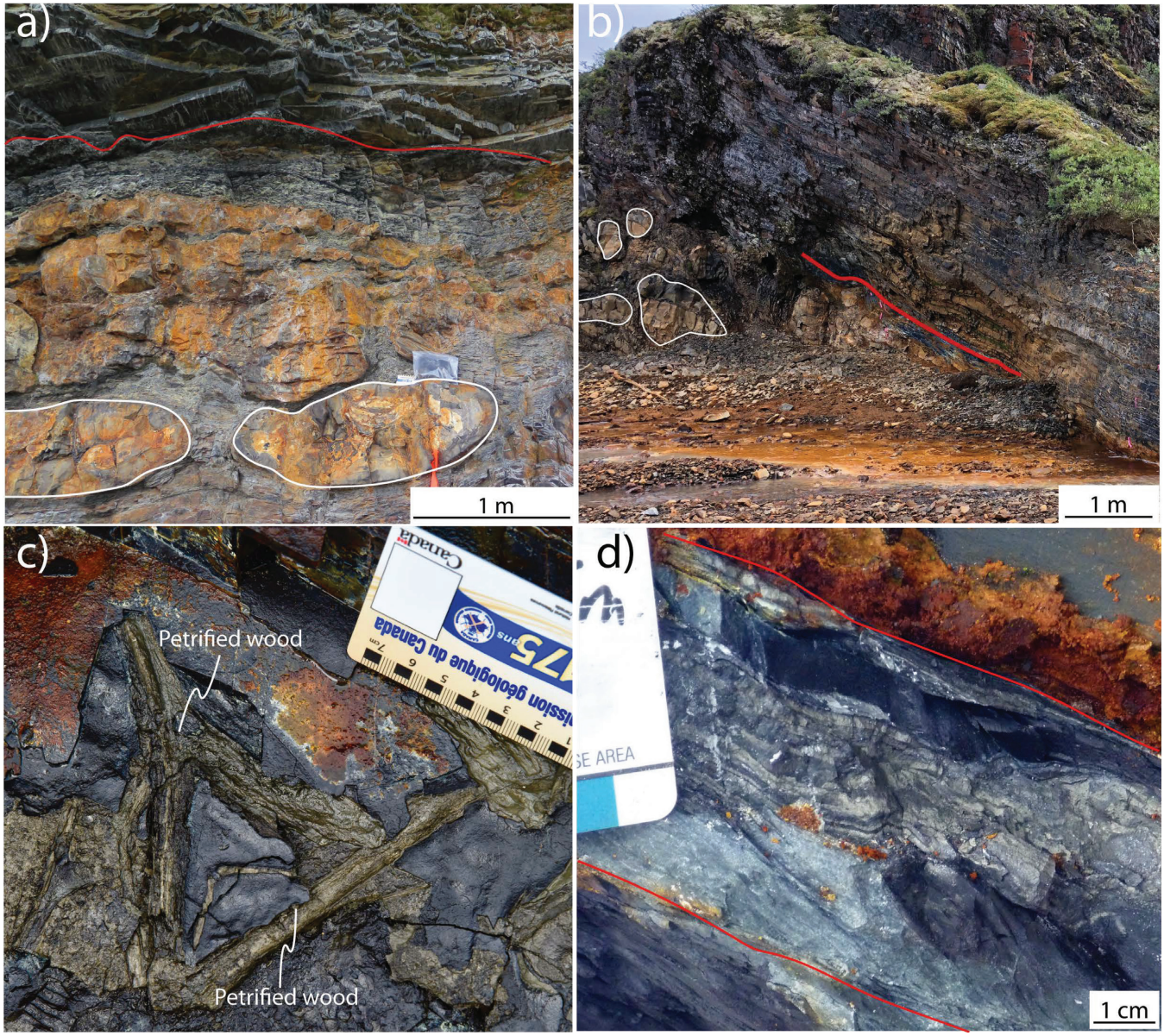

Figure 3. a), **b)** Photographs taken at the (a) Peel River and (b) Nick showings, Yukon, highlighting the relationship between concretion-bearing (outlined in white) Road River Group shales in contact with hyper-enriched black shale (HEBS; red line) and overlying Canol Formation rocks. NRCan photos 2020-131, 2020-132 **c)**, **d)** Close-up photographs of HEBS show (c) an exposed surface of HEBS containing pyrite-permineralized terrestrial flora at Peel River and (d) stratiform HEBS (outlined in red) interbedded with carbonaceous shales at Nick. NRCan photos 2020-133, 2020-134 (All photographs by J.M. Peter)

Kechika trough

The Kechika trough is the southern extension of the Selwyn Basin and is bounded by shallow-water autochthonous sedimentary rocks to the east (MacDonald Platform). To the west, the Kechika trough is bounded by the Tintina fault (Fig. 1). The Kechika trough is situated along the ancestral margin of the North American continent and contains late Cambrian to late Triassic clastic and carbonate rocks. Palinspastic restoration of the Kechika trough in the Middle to Late Devonian (time of HEBS formation; see Timing and Age of Mineralization, below) suggests it was an asymmetrical half-graben system measuring 30 to 40 km wide by at least 90 km (and probably 150–180 km) long (McClay et al., 1989).

The oldest rocks are Proterozoic to early Cambrian coarse grits of the Windemere Supergroup, and these are overlain by the Cambrian to Ordovician Kechika Group. The latter is an approximately 1.5 km thick succession of mudstone and limestone, with a few tuffs and felsic dykes. The Kechika Group is unconformably overlain by Ordovician to

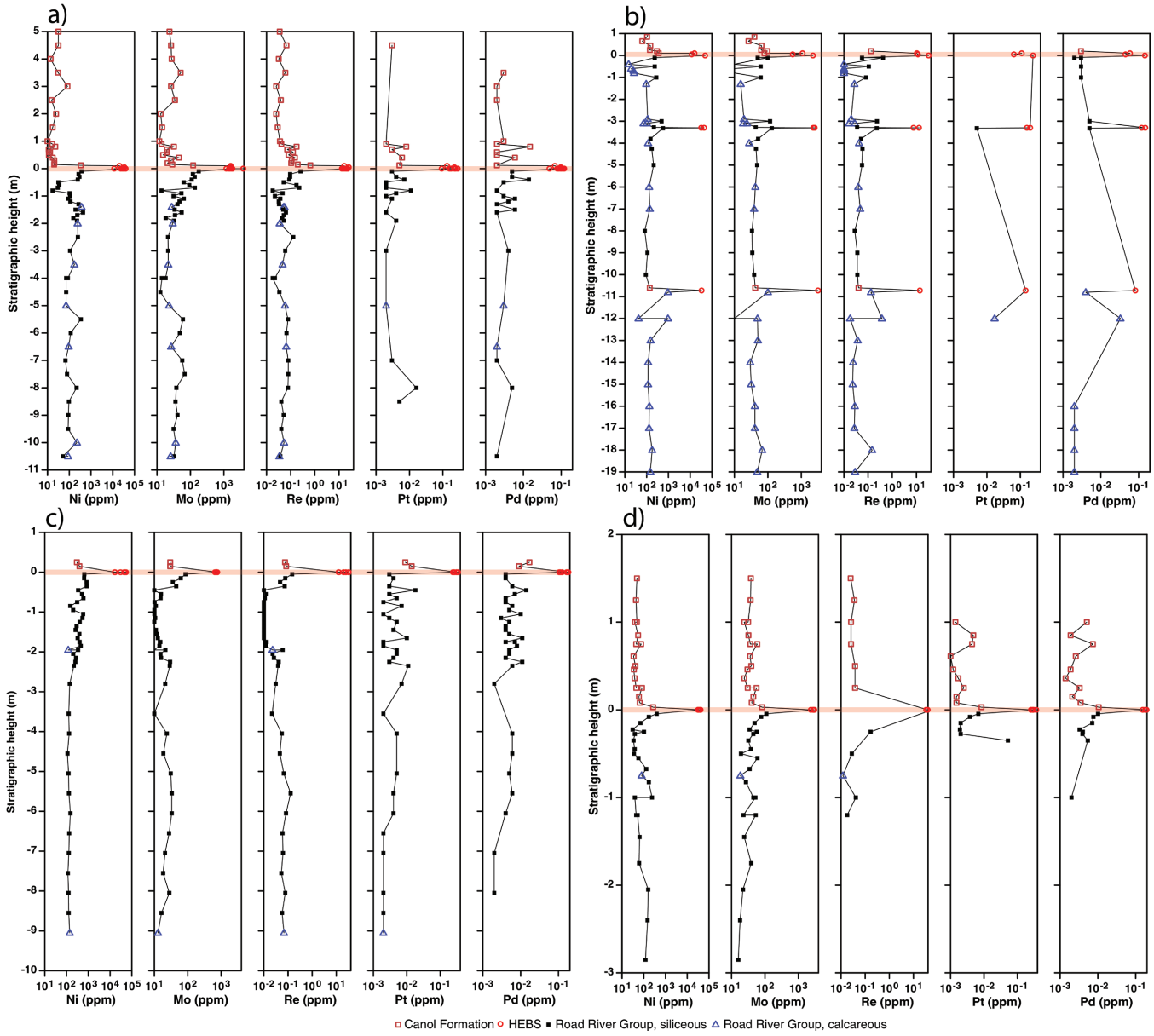

Figure 4. Bulk-rock trace-element geochemistry results of stratigraphic sections at the **a)** Peel River locality, **b)** Nick property, **c)** Monster River locality, and **d)** Moss locality, Yukon. The horizontal red line denotes the position of hyper-enriched black shale (HEBS) at the stratigraphic contact between the Road River Group and the Canol Formation.

Early Devonian clastic, carbonate, and volcanic rocks of the Road River Group, which represent the transition between platform and basin rocks.

The Road River Group occurs throughout the Kechika trough and has been informally subdivided into three units (MacIntyre, 1998): 1) Lower Road River group — interbedded siltstone, shale, limestone turbidites, and debris flows; 2) Ospika volcanics — mafic flows and sills interbedded with the lower Road River group; and 3) Upper Road River group — Silurian siltstone, underlying the Paul River Formation (deep-water marine turbidites: black chert, black shale, limestone debris flows, silty shale, and siltstone), which onlaps the Early to Middle Devonian Akie and Kwadacha reefs that consist of limestone and shale.

The Middle Devonian to Mississippian Earn Group overlies the reefs, and comprises carbonaceous and siliceous shale; argillite; phyllitic shale; and coarse, quartzose turbidites. The Earn Group is subdivided into three formations (Warneford, Akie, and Gunsteel) and collectively represents a major marine transgression that terminated reef growth and deposited sediments onto the MacDonald Platform. The Gunsteel Formation is the lowermost part of the Earn Group and consists of carbonaceous and siliceous shale, argillite,

and cherty argillite, with laminated pyrite and nodular barite in places. This formation hosts the Cardiac Creek (Akie) and other SEDEX deposits. The Akie Formation, comprising phyllic shale to silty shale and siltstone, overlies the Gunsteel Formation and forms the uppermost part of the Earn Group. The youngest rocks of the Earn Group are the Warneford Formation, which is intercalated with the Akie Formation and consists of chert pebble conglomerate, quartz wacke, and siltstone.

Immediately below the Gunsteel Formation is the Paul River formation, which comprises cherty shale, turbidite sequences, debris flows, and fossiliferous limestone. Underlying the Paul River formation are calcareous siltstones of the Road River Group (J.M. Peter et al., unpub. lithogeochemistry data, 2020).

LITHOSTRATIGRAPHY

Richards and Blackstone troughs

The lithostratigraphic sections at the Nick, Peel River, Moss, and Monster River HEBS localities are nearly identical, with only minor local lithological variations (Fig. 2b–e). A typical section comprises, from bottom to top:

1. a 2 to 20 m thick black shale with 1 to 1.5 m diameter calcareous concretions colloquially referred to as the 'limestone ball member' (Fig. 3a, b). Shale beds drape around concretions, and bedding is preserved within some concretions;
2. an up to 120 cm thick layer of siliceous, black shale with centimetre-scale barite and calcite nodules;
3. a 1 to 10 cm thick stratabound, stratiform semi-massive Ni-Zn-Fe-sulfide HEBS layer (Fig. 3c, d). Samples typically contain a number of sedimentary textures that include laminar bedding disrupted by soft-sediment deformation (Fig. 3d);
4. and black, siliceous shale to black cherty shale that is in sharp contact with the underlying HEBS mineralization.

The HEBS layers across northern Yukon possess striking enrichments in a broad suite of elements relative to the enclosing sedimentary rocks (Table 1; Fig. 4a–d). The enrichment occurs conspicuously at the regional stratigraphic contact between the Road River Group and Canol Formation, where HEBS mineralization is documented at each of the studied localities. Peel River is the only locality that is significantly different from the others in that three distinct HEBS layers have been documented there (Fig. 2c; Gadd et al., 2019b). These additional HEBS layers underlie the regional stratigraphic contact and are interbedded with carbonaceous shales of the Road River Group.

Akie property, Kechika trough

Hyper-enriched black shale mineralization on the Akie property has only recently been recognized; the account within this section is *after* Peter et al. (2018a; unpub. lithogeochemistry data, 2020). The HEBS on the Akie property is generally approximately 3 to 20 m stratigraphically below the base of the SEDEX mineralization (which occurs within the Gunsteel Formation of the Earn Group). The HEBS is broadly situated at the stratigraphic contact between the underlying Road River Group and the overlying Paul River formation, or within the latter, near its base. The HEBS has been intersected in exploration drill cores over a strike distance of approximately 5.5 km. There are differences in stratigraphic detail, depending on location on the Akie property. In the northwesternmost intersections (strata strike northwest-southeast), the HEBS forms a 10 to 20 cm true thickness (folded and deformed) layer within a deep-water cherty shale member. In the central intersections, the HEBS occurs within reef-marginal debris flows, and in the southeasternmost intersections, the HEBS occurs at the contact between underlying calcareous siltstone of the Road River Group and overlying fossiliferous Devonian Kwadacha limestone. In general, mineralization is 'weak' (disseminated), and not semi-massive to massive. The apparent differences in stratigraphic and textural detail can likely be explained by resedimentation of the HEBS in places; in most drill cores examined, the primary, non-resedimented HEBS occurs at the contact between the underlying calcareous siltstone and the immediate hanging wall is fossiliferous limestone of the Paul River formation (J.M. Peter et al., unpub. lithogeochemistry data, 2020).

LITHOGEOCHEMISTRY

Hyper-enriched black shale mineralization contains significant abundances of myriad elements, and the ranges and mean abundances of major, minor, and trace elements are presented in Table 1. The bulk compositions of the HEBS in Yukon are similar among localities. The most notable major elements are Ni, Fe, and S because these constitute the majority (by weight) of the HEBS. Notable minor (0.1–1 weight per cent) elements include Zn, As, Se, Mo, and Ba; their concentrations are moderately to significantly enriched compared to average upper continental crust (e.g. Rudnick and Gao, 2014). The concentrations of trace elements Sb, Re, Tl, Au, and PGE (particularly Pt and Pd) are also significantly enriched in HEBS. At Peel River, all of the HEBS layers are compositionally similar (Gadd et al., 2019b).

The lithogeochemistry of HEBS on the Akie property is somewhat different compared to HEBS from northern Yukon (Table 1). Although the metal enrichment suite in the HEBS on the Akie property (Ni, Zn, Se, As, Cu, Mo, Co, Re, Te, Pt, Pd, and Au) is strongly similar to that in the Yukon, the HEBS on the Akie property is generally more phosphatic and

calcareous with lower metal (Mo, Pt, Pd, Re, and Au) abundances than HEBS in Yukon. The compositional differences can be attributed to dilution by carbonate (eroded) from the ancient carbonate platform margin on the Akie property. The HEBS on the Akie property is also more enriched in Zn and Pb compared with Yukon HEBS, perhaps due to the close spatial relationship of the Cardiac Creek Pb-Zn deposit, and fluids responsible for the Cardiac Creek deposit may have overprinted or modified the composition and mineralogy of the Akie property HEBS (J.M. Peter et al., unpub. lithgeochemistry data, 2020).

MINERALOGY

Yukon

Hyper-enriched black shale mineralization is approximately 40 to 60 volume per cent sulfide minerals; the remainder comprises silicate minerals, phosphate minerals, and amorphous organic carbon (Hulbert et al., 1992; Gadd and Peter, 2018; Gadd et al., 2019b). The sulfide minerals within the HEBS are very fine grained mixtures of pyrite, Ni-sulfide minerals (millerite or vaesite), and sphalerite; discrete (pure) phases free of sulfide mineral inclusions are rare (Fig. 5a–f). This is especially true for millerite and vaesite, which nearly ubiquitously have pyrite and/or sphalerite inclusions. The predominant Ni-sulfide mineral in the HEBS at the Nick prospect is vaesite, whereas millerite is the predominant Ni-sulfide mineral at the other localities (Gadd and Peter, 2018). The nonsulfide mineralogy is fairly consistent among the studied localities, consisting of quartz, barite, apatite, and pyrobitumen with trace to minor hyalophane and K-feldspar (Gadd and Peter, 2018).

Pyrite in the HEBS layers has varied and complex textures, consisting of framboids (<0.003–0.1 mm in diameter) and minute crystallites (0.01–0.1 mm) within the mudstone matrix (i.e. matrix pyrite; Fig. 5a–c). Other pyritic features include replacements of organic remains (e.g. terrestrial plant matter; Fig. 5c) and nodules replete with silicate inclusions (Fig. 5d). Siliceous pyrite consists of very fine networks of anhedral pyrite interstitial to silicate minerals within the mudstone matrix (Fig. 5e); this pyrite variety occurs most commonly in close spatial proximity to millerite (Fig. 5e). A rare feature of the upper HEBS layer at Peel River is late-stage pyrite-marcasite veins (Fig. 5g). The veins comprise predominantly pyrite and marcasite, together with minor Ni- and As-enriched pyrite at the vein margins. The veins crosscut all bedded features within the mineralization, indicating that vein formation is the latest paragenetic event with respect to sulfide mineralization.

Vaesite and millerite also occur in several forms (Gadd and Peter, 2018; Gadd et al., 2019b). Most commonly, the Ni-sulfide minerals consist of anhedral, blebby masses that contain minute inclusions of matrix pyrite (Fig. 5a, b). The blebs occur in the mudstone matrix (Fig. 5a, b) and also encrust pyritic features (Fig. 5c, e). Euhedral millerite is associated with late quartz cement and is less common than anhedral forms (Fig. 5e).

Laser-ablation ICP-MS data reveal complex element distributions among sulfides (Fig. 6a–c). Pyrite is a significant sink for many trace elements, and its texture is an important control on trace-element composition (Gadd and Peter, 2018; Gadd et al., 2019b). The PGE host mineral is predominantly pyrite. Millerite is devoid of PGE (Fig. 6a, c), whereas vaesite is host to variable amounts (Fig. 6b). The incorporation of PGE into pyrite, from a paragenetic standpoint, is relatively early. This is established because (rare) late pyrite-marcasite veins free of PGE crosscut-bedded, PGE-bearing sulfides (Fig. 6c; Gadd et al., 2019b). Nickel (and Co-Zn-As-Cd-Sb; not shown) is enriched in the sulfide veins relative to the pyrite matrix (Fig. 6c), suggesting base metals were remobilized during late diagenetic fluid flow. The trace-element composition of pyrobitumen from Peel River and Nick has also been investigated and indicates that, although V, Zn, and Ni are moderately enriched and Re and Au occur in trace abundances, PGE are largely absent (Gadd et al., 2017; Henderson et al., 2019).

British Columbia

The mineralogy within the HEBS on the Akie property is similar, but not identical, to that in Yukon (Peter et al. 2018a; Gadd et al., work in progress, 2021; K. Haimbodi et al., unpub. mineral chemistry data, 2020). Sphalerite is more abundant than Ni-sulfide minerals, which include millerite (major), pentlandite (minor to trace), gersdorffite (trace), and violarite (trace). There are several textural varieties of pyrite present, including framboids, nodules, and replacements of organic remains (Peter et al., 2018a). Trace sulfide minerals include chalcopyrite, tennantite–tetrahedrite, galena, Se-rich galena, and clausthalite (PbSe). Gangue minerals consist of quartz, apatite, carbonate minerals, pyrobitumen, and aluminosilicates (and barite or other Ba-rich minerals). Much like HEBS in Yukon, the mineral textures reveal a complex paragenesis that suggests protracted sulfide mineralization that initiated early in the paragenetic history and extended into diagenesis (Gadd et al., work in progress, 2021). There are at least two textural varieties of both pyrite and sphalerite that indicate early diagenetic growth, and encrustations of millerite on these minerals suggests it formed paragenetically later. Additionally, the close proximity of the HEBS and overlying SEDEX mineralization suggests that the (later) Pb-Zn mineralizing fluids may have flowed diffusively through the HEBS in the footwall (Peter et al., 2018a).

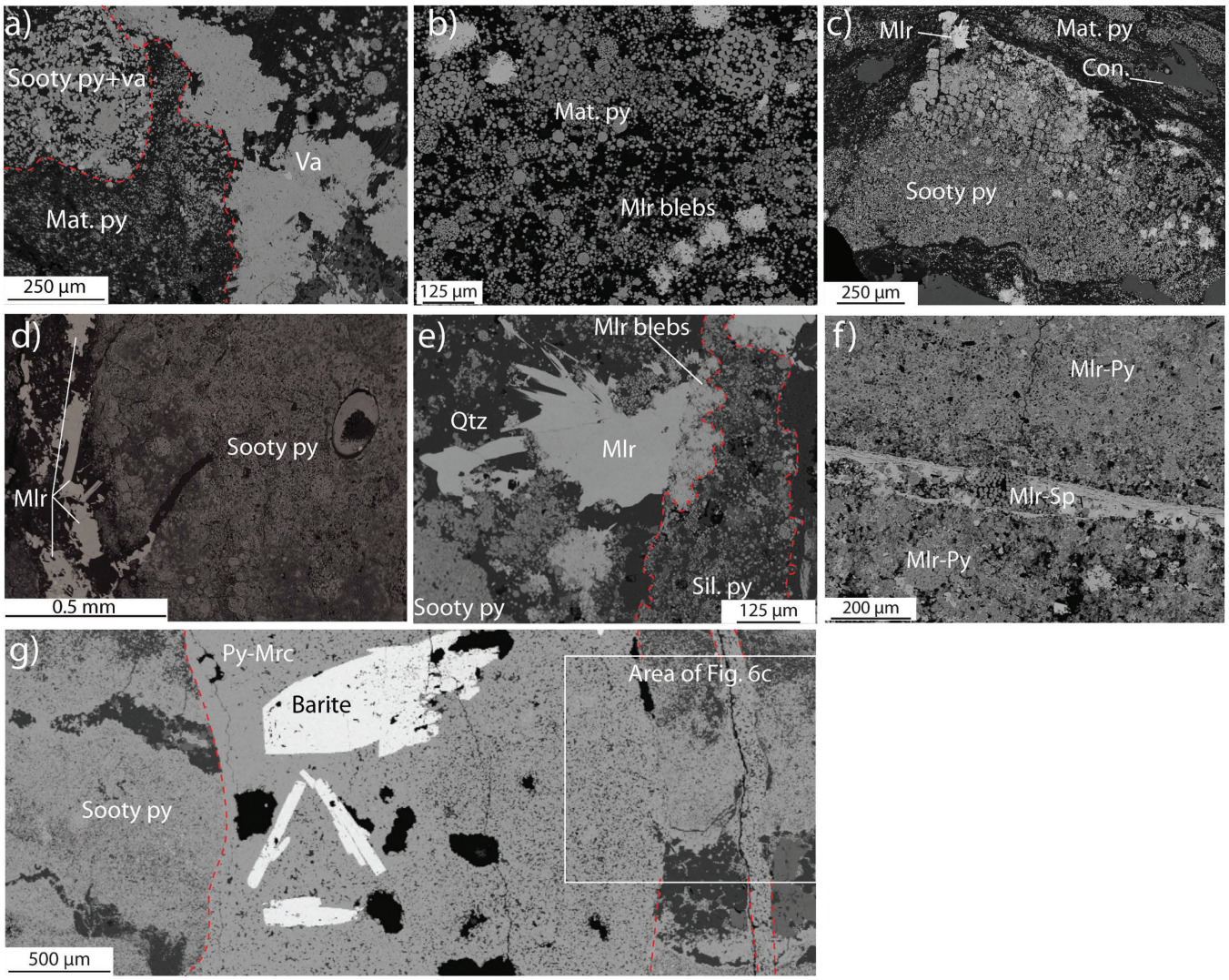

Figure 5. Backscattered-electron images of **a)** vaesite-pyrite mineralization from the Nick property consisting of relatively coarse- and fine-grained intergrowths of vaesite and pyrite with disseminated pyrite in the mudstone matrix (sample Nick89-11); **b)** fine-grained, variable-diameter framboidal pyrite within mudstone matrix and anhedral millerite blebs (sample 17-POA-072, Peel River); **c)** sooty pyrite replacing carbonaceous material from terrestrial flora with a millerite rim at the outer margin; a small, indeterminate conodont fragment within the mudstone matrix is also visible (sample 17-POA-049b, Peel River); **d)** sooty pyrite mantled by subhedral to euhedral millerite (sample WDG94-ss, Monster River); **e)** euhedral, acicular millerite and anhedral millerite blebs adjacent to cryptocrystalline pyrite within siliceous matrix and sooty pyrite (sample WDG08-02-01c, Peel River); **f)** a very fine grained mixture of pyrite and millerite that is crosscut by a bedding-parallel millerite-sphalerite vein (sample 17-POA-072, Peel River); and **g)** bedding-parallel sooty pyrite crosscut by a vein of pyrite, marcasite, and euhedral barite (sample 17-POA-055a, Peel River). Dashed red lines have been added to highlight separate mineralogical features (*modified after* Gadd and Peter, 2018; Gadd et al., 2019b). Abbreviations: Con.: conodont fragment; Mat. py: matrix pyrite; Mlr: millerite; Mrc: marcasite; Py: pyrite; Qtz: quartz; Sil. py: siliceous pyrite; Sp: sphalerite; Va: vaesite.

TIMING AND AGE OF MINERALIZATION

An early application of Re-Os geochronology in black shales determined a Devonian age (380–367 Ma) for Nick prospect HEBS mineralization (Horan et al., 1994). The broad age range agreed with established stratigraphic relationships but since Horan et al. (1994) was completed, Re-Os geochronology methods have allowed for much greater analytical precision (Stein, 2014). New Re-Os geochronological analyses using more refined methods than Horan et al. (1994) give isochron ages of 387.5 ± 4.4 and 390.7 ± 5.1 Ma for the Peel River and Nick HEBS, respectively (Gadd et al., 2020). Geochronology of HEBS from the Moss locality (389.4 ± 5.7 Ma; Gadd et al., unpub. data, 2021) is consistent with the other localities, indicating that mineralization ages are identical, within error, and that the Moss locality is coeval with Peel River and Nick.

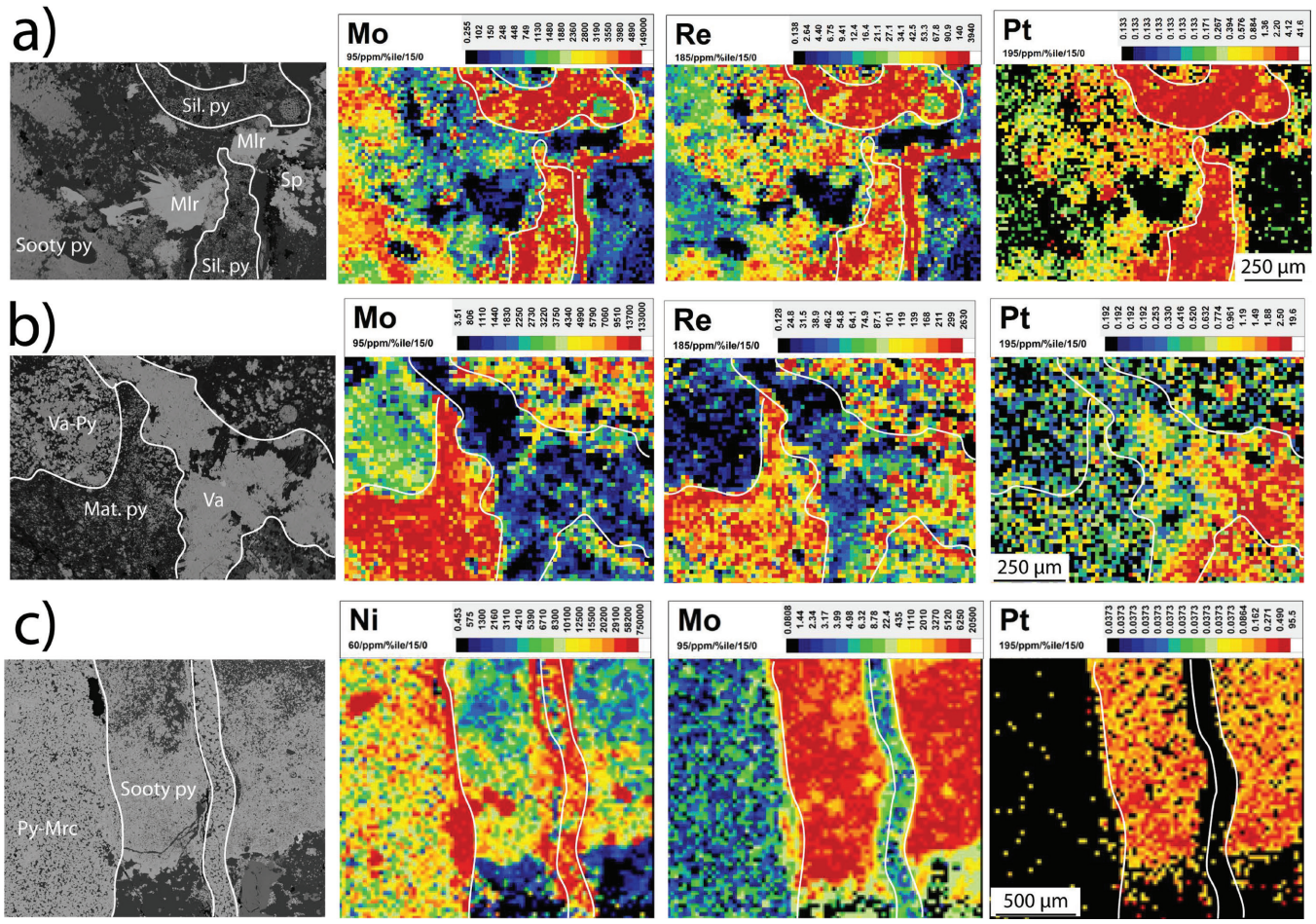

Figure 6. Backscattered-electron (BSE) images and corresponding laser-ablation inductively coupled plasma mass spectrometry (LA-ICP-MS) raster maps with mineralization in parts per million, from the Nick property and Peel River locality, Yukon: **a)** millerite-pyrite-sphalerite mineralization from the Peel River locality (sample WDG08-02-01c) and corresponding LA-ICP-MS maps of Mo, Re, and Pt. Cryptocrystalline pyrite is outlined in white to highlight where these elements are concentrated; **b)** vaesite-pyrite mineralization from the Nick property (sample Nick89-11) and corresponding LA-ICP-MS maps of Mo, Re, and Pt. Vaesite is outlined in white to emphasize relative distributions of elements between pyrite and vaesite; **c)** a late pyrite-marcasite vein cross-cutting younger diagenetic pyrite from Peel River (sample 17-POA-055a) and corresponding LA-ICP-MS maps of Ni, Mo, and Pt (*modified after* Gadd and Peter, 2018; Gadd et al., 2019b). The vein contacts are outlined in white. Abbreviations: Mrc: marcasite; Mlr: millerite; Py: pyrite; Sil. Py: siliceous pyrite; Sp: sphalerite; Va: vaesite.

Conodonts from the immediate host rocks at Peel River give an overall age range of 388.6 to 385.4 Ma, indicating a maximum timeframe of approximately 3 Ma for the accumulation of the 2 m of sediment that includes HEBS (Gadd et al., 2020). Conodonts collected 1.2 to 1.9 m below the HEBS at the Nick prospect yield a narrower age range (389.2–387.7 Ma; a 1.5 Ma time interval) that is well within the isochron range; however, the HEBS must be younger than the underlying sediments from which the conodont elements were extracted. At Monster River, the westernmost HEBS locality studied in Yukon (Fig. 1), conodonts recovered from the mineralization are within the *Polygnathus ensensis* zone (388.2 Ma) up to the *P. ansatus zone* (386.3 Ma; S. Gouwy, unpub. conodont data, 2019), indicating an identical age range to the HEBS from the Peel River prospect. There are no age constraints for the Moss showing; however, given the consistency of age relationships at the stratigraphic contact between the Road River Group and Canol Formation, and because the Moss prospect HEBS is located at this contact, it is highly probable that the HEBS mineralization was a contemporaneous, basin-scale event within the Middle Devonian. On the Akie property, conodonts collected from carbonate strata 6 m above the HEBS span the *P. australis* (389.2 Ma) to *P. ansatus* zones, indicating that the HEBS pre-dates *P. ansatus*. Gadd et al. (2020) interpreted the closeness in age of strata on the Akie property and HEBS in Yukon to reflect basin-scale mineralization; moreover, the close agreement between isochron ages for the semi-massive sulfides and the conodont ages signifies that mineralization was synchronous with sedimentation.

DEPOSITIONAL ENVIRONMENT

Understanding the ambient paleoenvironmental conditions is critical to elucidating the genesis of these deposits because HEBS formation was synchronous with sedimentation. The research on HEBS has taken a multifaceted approach to this by applying traditional (e.g. lithogeochemical; Crawford et al., 2019; Gadd et al., 2019a; Gadd, Peter, Fraser et al., this volume) and non-traditional (e.g. metal stable isotopes; Crawford et al., 2019) analytical geochemical methods. To define the paleoredox of the environment within which the HEBS was deposited, it is important to compare both mineralized and barren (unmineralized) samples throughout the stratigraphic succession because reduction-oxidation (redox) fluctuations may have played an important role in 'priming' the environment that ultimately promoted the accumulation and preservation of semi-massive sulfides.

Several paleoredox proxies based on bulk geochemical composition have been developed that can be applied to ancient sedimentary successions. Many of these are equivocal and provide contradictory results (*see* Peter et al., 2018b). This is certainly the case for HEBS in Yukon. Cerium anomalies (Ce-Ce*) are consistently less than 1, but fluctuate in the Road River Group (Table 1). These values progressively decrease within the vicinity of HEBS (approximately 1 m) to reach minima within the HEBS of the studied localities (Crawford et al., 2019; Gadd et al., 2019a; Gadd, Peter, Fraser et al., this volume). This suggests that the ambient environment became progressively oxygenated up to and during HEBS formation. Concomitant increasing Mo abundances, with maxima in the HEBS, suggest the opposite because Mo is sequestered in anoxic to euxinic environments much more readily than in oxygenated ones (Tribovillard et al., 2006; Scott and Lyons, 2012). The ambient conditions during HEBS formation are, therefore, somewhat counterintuitive because the HEBS consist of semi-massive sulfides that could only have formed under reducing conditions; however, uniformly negative Ce-Ce* (Table 1) suggest that suboxic conditions were prevalent. We interpret the contradictory Ce-Ce* and Mo abundances to reflect a high degree of redox stratification in the immediate environment in which the HEBS formed (i.e. in the water column, and on/within the immediate seafloor muds).

The terrigenous input (TIP; $Na_2O + Al_2O_3 + K_2O + TiO_2$) to the HEBS bulk compositional makeup is extremely low (Table 1), indicating that there was little clastic detrital sedimentation. This characteristic is in keeping with one of the primary controls on HEBS formation in Yukon: clastic sediment starvation (Lehmann et al., 2016; Gadd and Peter, 2018; Pagès et al., 2018; Gadd et al., 2019a, 2020; Gadd, Peter, Fraser et al., this volume). Nevertheless, detrital minerals and/or biogenic debris sinking through a redox-stratified water column and settling on the seafloor may have acquired a negative Ce-Ce* from the suboxic seawater they travelled through, prior to settling on/in the reducing environment of the muds at the seafloor. The consistently high Si abundances in the Canol Formation likely represent high degrees of paleoproductivity (radiolarian blooms), and the stratigraphically upward decreasing Ce-Ce* probably reflect basin ventilation associated with the incursion of nutrient-rich (oxygenated) waters. Alternatively, as previously suggested, the negative Ce-Ce* may reflect a high degree of open marine deposition (Murray et al., 1990; Murray, 1994).

METAL SOURCES AND BASINAL PROCESSES

The critical drivers of mineralization and sources of metals for HEBS are unknown and the theories remain controversial. This is because there are few clues preserved as to the absolute causes of mineralization, many of the metals that constitute HEBS are uncommon (or do not commonly occur together), and mineralization is geographically widespread. Two prevailing hypotheses have been developed to explain the salient features of HEBS mineralization: 1) precipitation from hydrothermal fluids vented at the seafloor and 2) direct precipitation of metals from ambient seawater. The first hypothesis proposes that metals are sourced through the flow of hydrothermal (and possibly hydrocarbon or basinal) fluids along synsedimentary growth faults (Coveney et al., 1992; Emsbo et al., 2005; Henderson et al., 2019). The second hypothesis proposes that combined organic matter remineralization, low clastic sedimentation rates, and effective chemical trapping promoted the accumulation and preservation of sulfide minerals (Lehmann et al., 2007). Metal deposition may have been further enhanced by high primary productivity (Lehmann et al., 2016; Yin et al., 2017) and/or Fe-Mn–oxyhydroxide particulate shuttling (Gadd et al., 2019; Gadd, Peter, Fraser et al., this volume).

In the hydrothermal model, metalliferous fluids escape from conduits and are trapped, either physically (saline brines in depressions) or chemically (sulfidic, carbonaceous sediments). At the Nick prospect, discordant 3 m wide pyrobitumen veins have been interpreted to be the conduits for fluid transmission (Hulbert et al., 1992). The pyrobitumen vein near the Nick prospect is metalliferous and contains minor abundances (hundreds to thousands of parts per million) of Ni, Zn, and V (Hulbert et al., 1992; Henderson et al., 2019), and pyrobitumen in HEBS from the Peel River prospect possess similar abundances of Ni, Zn, and V (Gadd et al., 2017; Henderson et al., 2019); however, the role of pyrobitumen (or a liquid hydrocarbon precursor) as the metal-bearing transport medium is uncertain. Although the pyrobitumen is metalliferous, the scale at which hydrocarbon transport of metals operated is unknown. It also is unclear how a single, basin-scale hydrothermal event could account for mineralization at all of the localities. Coeval HEBS localities at the regional Road River Group–Canol Formation stratigraphic contact are scattered across northern Yukon, but only at Nick has a feature been found that resembles a feeder system.

The role of high-temperature fluids (relative to ambient seawater) is difficult to assess directly because fluid-inclusion trapping temperatures cannot be measured in the fine-grained sulfide minerals. Indirect, qualitative temperature assessments are possible using geochemical proxies (e.g. Eu anomalies; Eu-Eu*). Positive Eu anomalies (i.e. Eu-Eu* >1) in marine environments typically form by precipitation from hot (100–250˚C), reducing, acidic seafloor hydrothermal vent fluids (Sverjensky, 1984; Douville et al., 1999). To a lesser extent, positive Eu anomalies may form in low-temperature environments that are highly alkaline and reducing (e.g. anoxic porewaters) and may be preserved in authigenic carbonate minerals (Sverjensky, 1984; Schuster et al., 2018). Hyper-enriched black shale mineralization lacks positive Eu anomalies (average = 0.99 ± 0.13; Table 1). This suggests metalliferous fluids responsible for HEBS mineralization were not high-temperature seafloor vent fluids. Unmineralized host black shales have weakly negative to weakly positive Eu-Eu* (Table 1) that we interpret to reflect clastic detrital input (Gadd et al., 2019a), whereas more positive values are attributed to contributions from authigenic phases (e.g. carbonate minerals; Shuster et al., 2018). Indeed, the highly reducing, alkaline environment within which the carbonate concretions precipitated would have promoted the development of positive Eu-Eu* (Gadd et al., 2019a).

In the absence of high-temperature hydrothermal fluids, elemental enrichment may originate from ambient seawater within a favourable sedimentary environment. Determining the significance of these processes can be achieved by using different geochemical criteria. For example, a major component of the HEBS is the abundance of S (Table 1; principally in sulfide minerals). The bulk S isotope compositions in HEBS samples from Peel River, Moss, and Nick are exclusively negative (–30 to –10‰; Hulbert et al., 1992; Gadd et al., 2019a; M.G. Gadd unpub. S isotope data, 2018). Negative bulk sulfur isotope compositions signify that reduced sulfur was generated by bacterial sulfate reduction in an open system (i.e. no Rayleigh fractionation; Goldhaber and Kaplan, 1980; Goodfellow, 1987). Bacterial sulfate reduction is the process by which microbes consume labile organic matter through dissolved sulfate respiration. The byproducts of this anaerobic reaction are CO_2 and H_2S, and this process is restricted to anoxic environments such as below the chemocline in an oxygenated water column (Goldhaber and Kaplan, 1980). In the presence of dissolved metals or reactive particles, the reduced sulfur may be fixed as metal sulfide minerals; within HEBS, these are most commonly pyrite, vaesite or millerite, and sphalerite (Fig. 6a–c). Sulfate-reducing microbes operate most effectively at low temperatures (Sokolova, 2010) and cease to metabolize at temperatures above approximately 100˚C (Jørgensen et al., 1992; Machel, 2001); this constraint provides further evidence that reduced sulfur generation for HEBS occurred in a low-temperature environment.

Initial Os (Os_i) ratios are a powerful tool that can be used to delineate different sources of Os in seawater, and the principal fluxes to seawater are unradiogenic mantle and meteorites (Os_i = 0.127) and radiogenic continental crust (Os_i > 0.127–1.9; Cohen, 2004). Gadd et al. (2020) report Os_i ratios at Peel River (Os_i = 0.25 ± 0.07) and Nick (Os_i = 0.32 ± 0.20), and the initial Os ratios of unmineralized black shales from both Peel River and Nick together with the HEBS define an isochron. Gadd et al. (2020) interpreted this to reflect a shared source of Re and Os between HEBS and unmineralized shale. These values are comparable to Middle Devonian seawater (0.262 ± 0.034; Miller, 2004), as determined by Re-Os geochronology on Givetian organic matter from the Western Canadian Sedimentary Basin. The overlapping Os_i ratios of HEBS, unmineralized shale, and Givetian organic matter suggest a seawater source for these metals. Congruency between the topologies of continental-crust–normalized PGE profiles for seawater and HEBS is additional evidence to support a seawater metal source (Lehmann et al., 2016). Indeed, there is broad congruency among the patterns from different localities (Fig. 7). Hyper-enriched black shale from China also possesses similar PGE profiles compared with seawater, which suggests a common seawater origin (Fig. 7; Xu et al., 2011, 2013; Lehmann et al., 2016).

Lehmann et al. (2016) advocate that bio-essential nutrient trace elements bound to organic matter were primarily responsible for hydrogenous export to the seafloor in the case of HEBS deposits in China. Modelling metal accumulation related to primary productivity from the modern Cariaco Basin, Venezuela (a restricted, euxinic basin) underpins the hydrogenous metal hypothesis for the HEBS in China, wherein extremely efficient organic carbon remineralization combined with minimal clastic sedimentation facilitated vast metal accumulations (Lehmann et al., 2016; Johnson et al., 2017). The configuration of the Richardson trough (Fig. 1) is favourable for restriction or periodic restriction depending on eustatic sea-level changes (Fig. 8a, b; Fraser and Hutchison, 2017). The high abundances of total organic carbon (TOC) in host rocks and HEBS, combined with evidence for suboxic marine conditions, suggest that the basinal environment was highly biologically productive (Piper and Calvert, 2009); however, exceptional preservation cannot be ruled out because the marine environment of the Richardson trough has also been interpreted to be redox stratified (Fig. 8a, b; Fraser and Hutchison, 2017; Gadd et al., 2019a; Gadd, Peter, Fraser et al., this volume).

Henderson et al. (2019) argued that the high degree of metal enrichment (many orders of magnitude higher than metal concentrations in seawater) cannot solely be derived from organic matter remineralization, but must also come from another source. It is possible that metal export to the seafloor was fueled by hydrogenous Fe-Mn–oxyhydroxide particulate shuttle activity, in addition to a

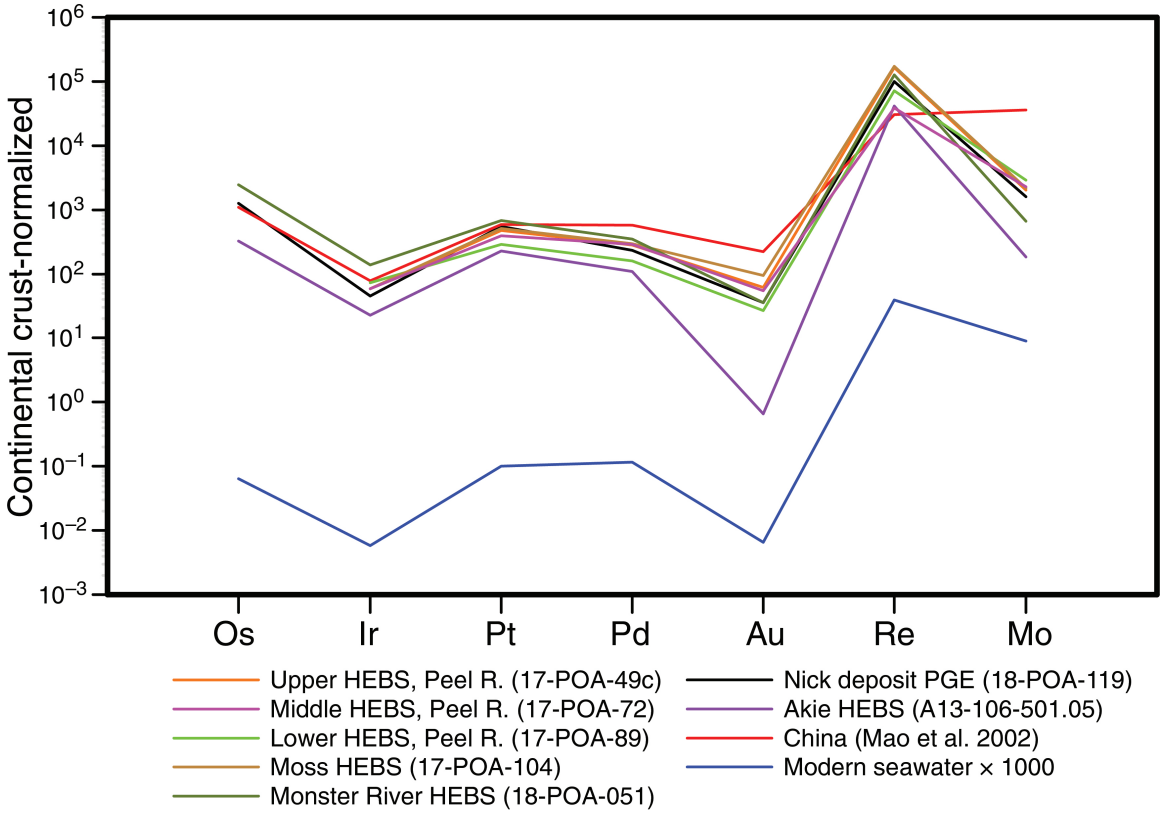

Figure 7. Upper-continental-crust–normalized platinum-group elements, Au, Mo, and Re contents (Rudnick and Gao, 2014) of modern seawater (Nozaki, 1997) and hyper-enriched black shale (HEBS) layers from Peel River, Nick, Moss, and Monster River, Yukon; Akie property, British Columbia; and China (Mao et al., 2002).

high flux of organic carbon (Fig. 8c). Ferromanganese oxyhydroxides commonly coprecipitate in oxygenated marine environments and sequester a diverse range of hydrogenous elements (Koschinsky and Hein, 2017). Shuttling occurs when these Fe-Mn–oxyhydroxide particulates form in an oxygenated environment and scavenge metals as they settle through the water column and are deposited at the seafloor (Dellwig et al., 2010). Particulate shuttling can effectively deliver myriad hydrogenous trace metals (in addition to Fe and Mn) to the seafloor together with the particulates (Koschinsky and Hein, 2017). Gadd et al. (2019a; Gadd, Peter, Fraser et al., this volume) show that particulate shuttling was active prior to, during, and after HEBS formation, and suggest that Fe-Mn–oxyhydroxide particulate shuttling contributed elements to the HEBS, which is supported by the extremely high Fe abundances; however, a lingering question concerns the role of Mn oxyhydroxides and their ultimate fate. Manganese is only present in trace amounts within the HEBS and its host rocks. Our model assumes that Mn oxyhydroxides reductively dissolve within an environment capable of preserving Fe oxyhydroxides. The model also assumes that Fe-oxyhydroxide particles are shuttled to the seafloor, where they reductively dissolve in the presence of sulfide to form pyrite (Fig. 8d). It may be that Mn did not (or could not) reprecipitate into stable phase(s) within the ambient paleoenvironment.

Crawford et al. (2019) presented Mo and Tl isotopic data from the Peel River HEBS and host rocks (Fig. 1) that provide evidence for a seawater source for these metals. The strongly negative Tl isotope compositions of the HEBS do not match any known hydrothermal Tl reservoirs and are more similar to values for sedimentary pyrites that have reductively sequestered metals (Nielsen et al., 2011). The negative Mo isotope compositions of the HEBS similarly do not reflect marine hydrothermal processes, but rather suggest sequestration of Mo by an intense Fe-oxyhydroxide particulate shuttle (cf. Scholz et al., 2017).

In ancient sedimentary rocks, the role of particulate shuttling may be assessed by comparing enrichments of authigenic Mo and authigenic U. The enrichment of redox-sensitive authigenic trace elements originates during sedimentation by precipitation or recrystallization; to calculate this, the abundance is normalized to the abundance of a solely detrital element, such as aluminum, present in the same sample, and normalized to the element of interest in post-Archean Australian shale (Algeo and Tribovillard, 2009). Authigenic enrichments of these elements provide insights into the marine cycling of these redox-sensitive trace elements (Tribovillard et al., 2012; Cheng et al., 2016).

Fraser and Hutchison (2017) present authigenic Mo and U data for time-stratigraphically equivalent rocks at Trail River in the eastern Richardson Mountains, where there is strong evidence that a particulate shuttle operated in the water column during deposition of the Canol Formation. Kabanov (2019) presents authigenic Mo and U data for age-equivalent, correlative rocks on the Mackenzie platform that also indicate the presence of an active particulate shuttle. The sedimentary rocks at both of these regional localities do not possess the magnitude of metal enrichment evident within HEBS; however, the data indicate that particulate shuttling was a basinwide phenomenon that extended from the drowned carbonate platform into the sediment-starved basin. This basin-scale particulate shuttle was perhaps the most active during the time of HEBS formation, during which extremely high abundances of elements were concentrated in a thin layer. Particulate shuttling persisted well into the deposition of the Canol Formation (Fraser and Hutchison, 2017; Kabanov, 2019).

REGIONAL AND GLOBAL CONSIDERATIONS

Metal enrichment in Middle Devonian black shales is a prominent feature not only in the northern Canadian Cordillera, but also globally. In the eastern Richardson Mountains, the shales that compose the stratigraphic contact of the Road River Group and Canol Formation are enriched in a similar suite of elements to those in the HEBS (e.g. Ni, Mo, Se; Fraser and Hutchison, 2017). The absolute abundances are not as high as in the HEBS, but the enrichment is noteworthy given its correlation with the HEBS 40 km to the west. The HEBS at the Cardiac Creek Zn-Pb-Ag deposit in Kechika trough (Fig. 1) are approximately the same age as those in Yukon (Gadd et al., 2020), indicating that HEBS formation during the Middle Devonian may have occurred along the extent of the Laurentian continental margin. Elsewhere, the Eifelian–Givetian stage boundary at Jebel Mech Irdane, Morocco, contains pyritic beds (Walliser et al., 1995) with enrichments (albeit abundances lower than HEBS) of redox-sensitive trace elements (e.g. Ni, V, Mo, As; Ellwood et al., 2003) and PGE (Schmitz et al., 2006); these enrichments may be temporally linked to HEBS precipitation in the northern Canadian Cordillera.

An auspicious basin configuration likely promoted the formation and preservation of HEBS in the studied area. The Richardson trough, where these shales were deposited, has been interpreted as an aulacogen (Cecile et al., 1997), and plate reconstructions indicate that it was bound to the east by the Mackenzie platform and to the west by the Yukon block (Lane, 2007). Carbonate buildups apparently also occurred on the southern margin, but the northern margin in the Middle Devonian is not well defined (Cecile et al., 1997). Thus, the Richardson trough likely underwent periodic restriction (Fig. 8a), especially during sea-level lowstands such as during the late Lower Devonian (Haq and Schutter, 2008; Fraser and Hutchison, 2017). Global-scale sea-level rise during the Middle Devonian flooded the carbonate platforms and resulted in widespread black shale deposition (e.g. the Canol Formation; Lane, 2007). This probably facilitated the connection of previously restricted basinal environments with oxygenated seawater, which provided critical nutrient input (Fig. 8b) and resultant biomass export to the seafloor (Lehmann et al., 2016). Although the Blackstone trough is less studied than the Richardson trough, it is contiguous with it (Fig. 1; Norris, 1997). Thus, it stands to reason that the same events affected both troughs similarly. Because HEBS are positioned in troughs along the continental margin, it is likely that nutrient-rich upwelling fueled primary productivity of radiolarians and massive carbon export to the seafloor; favourable basin architecture led to the accumulation of the organic matter, which sustained bacterial sulfate reduction within the seafloor environment.

Linked periodic restriction and ventilation in continent-marginal troughs is a key aspect in the formation and preservation of HEBS. Sea-level instability during the Middle Devonian is well documented, and this may have contributed to the prominent biotic crises during this period (Brett et al., 2018). The Re-Os and biostratigraphic age constraints for the HEBS overlap with the Kačák, *P. pumilio*, and Taghanic biotic events (Becker et al., 2012; McGhee et al., 2013; Narkiewicz et al., 2016; Brett et al., 2018). These events had a global extent and may have initiated a prolonged period of decline in biodiversity (Fan et al., 2020). Key aspects include abrupt faunal changes, eustatic sea-level rise, continental shelf flooding, and black shale deposition (House, 1996, 2002; Haq and Schutter, 2008; Becker et al., 2012; Brett et al., 2018). We hypothesize that metal enrichment may be a hallmark feature of Middle Devonian eustatic/biotic events. Our age constraints are insufficiently precise to implicate a particular event; however, the conspicuous overlap in time between HEBS formation and global-scale biotic crises suggests that eustatic sea-level rise may have been an important aspect of basin-scale HEBS mineralization. Eustatic sea-level rise would have reconnected the restricted marginal troughs with open-marine waters and provided steady-state input of nutrient and other trace elements in seawater. It is possible that this occurred over long durations in a setting with little clastic input within favourable basinal positions (e.g. semi-restricted sub-basins) on the western Laurentian continental margin.

IMPLICATIONS FOR EXPLORATION

The ages of HEBS mineralization in north Yukon and northeastern British Columbia (located more than 1000 km apart) are the same or closely similar. The mineralization is hosted by a continuous belt of Middle Paleozoic passive margin sedimentary rocks, suggesting that there is significant potential for additional discoveries. Although HEBS occurrences are typically thin, the high abundances of elements

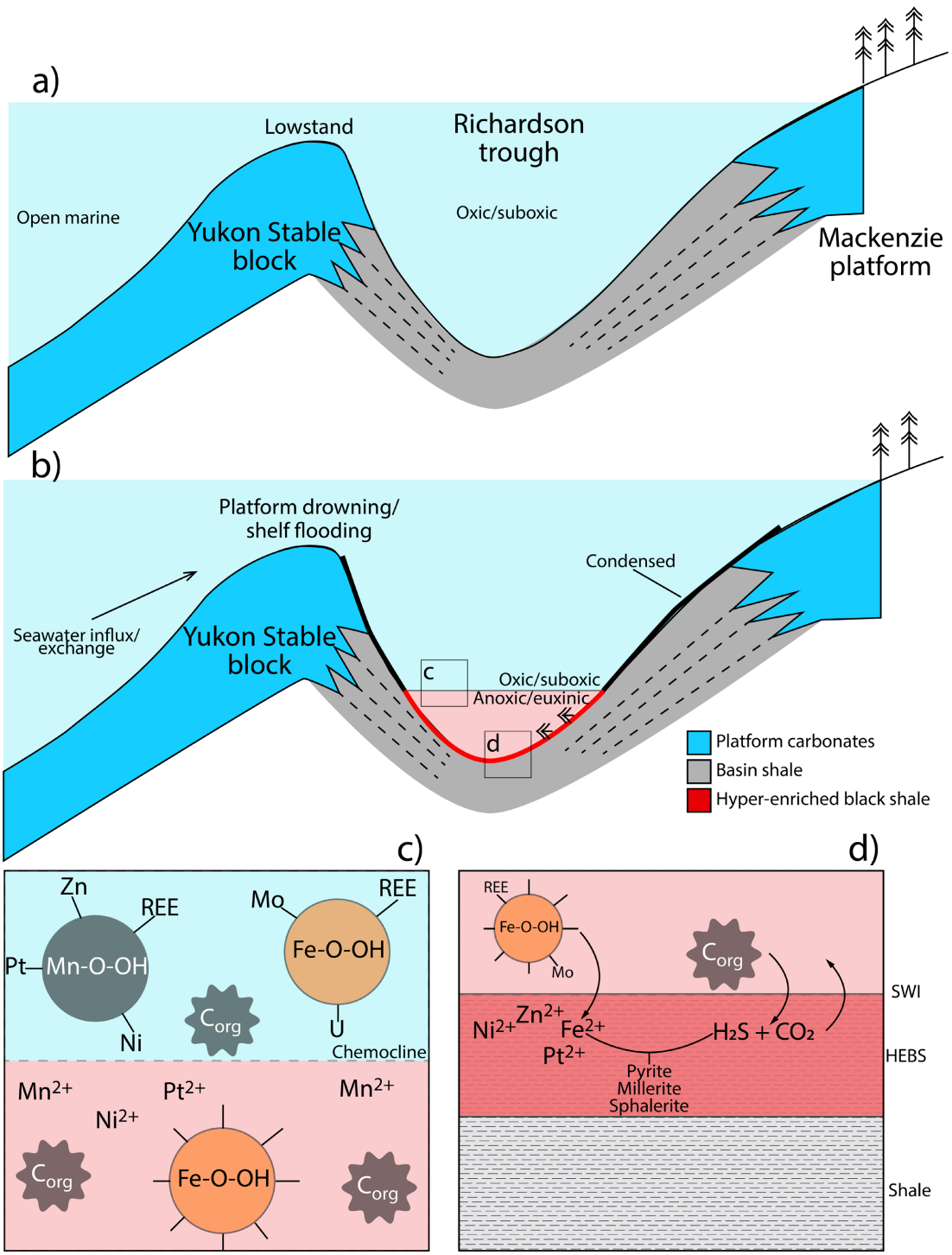

Figure 8. Cartoon schematic (not to scale) showing the relationship of hyper-enriched black shale (HEBS) formation in the Richardson trough to **a)** regressive and b) transgressive eustatic sea-level changes (*modified from* Fraser and Hutchison, 2017). The Richardson trough is restricted during sea-level lowstands (pre-Eifelian) and flooded during highstands (upper Eifelian to Givetian). Platform drowning and shelf flooding results in deposition of widespread condensed sedimentary horizons (black line), including polymetallic HEBS (red line). Above **c)** the chemocline between partially oxygenated (suboxic) and anoxic/euxinic basinal redox conditions, Mn-oxyhydroxide particulates are stable, but they dissolve in the absence of oxygen, releasing metals bound to these particles. Iron oxyhydroxide particulates are stable over a much wider range of oxygen-poor conditions and do not dissolve until reaching the sediment-water interface (SWI), where **d)** particulate C_{org} and Fe deposition and dissolution occurs at or near the sediment-water interface. Reductive dissolution of Fe particulates and bacterial sulfate reduction via organic matter respiration fuel sulfide precipitation within sediment porewaters. This figure presents the HEBS layer as a blanket that covers the seafloor of the Richardson trough; however, it is unclear whether HEBS actually blankets the seafloor or only forms a 'bathtub ring' at the margins.

(some of high economic value such as PGE, Au, and Re) within them make them attractive exploration targets. Many of the elements present are considered critical because they have limited supply chains, as well as applications in modern society and green technologies.

There may be paleoceanographic controls on HEBS mineralization. The Moss, Peel River, and Nick localities are within the confines of the Richardson trough; Monster River is within the Blackstone trough; and the Akie property is within the Kechika trough. Thus, there is circumstantial evidence to indicate that the trough settings (within the overall Selwyn Basin) imparted an additional salient control on HEBS. The stable blocks flanking these troughs may have served as effective high-standing weirs that (partly to completely) prevented the unrestricted flow and incursion of fresh seawater into the trough. Only during discrete sea-level rise (and for a restricted period of time) could fresh batches of seawater have entered the troughs; this seawater likely provided the metals for HEBS. The restricted setting of the troughs may also have promoted the requisite redox conditions in the water column and subsurface muds necessary for HEBS formation (Fig. 8).

The HEBS in the northern Canadian Cordillera display no regular or systematic spatial-temporal relationship to magmatism or magmatic products (e.g. plutons, volcanic flows, or large igneous provinces). Despite the geographically widespread distribution of HEBS, the deposits have no associated hydrothermal alteration and, therefore, will not have an enlarged footprint (i.e. beyond the limits of the mineralization). In the field, HEBS can be difficult to identify due to its occurrence in thin layers and its dark colour similar to the surrounding host rocks; however, its occurrence is probably most readily signalled by a close proximity (<2 m stratigraphically below) to black shale with large carbonate concretions (up to 1.5 m in diameter; Fig. 3a, b). The thin HEBS layers weather recessively, and weathered samples commonly have whitish-green to light green secondary mineralization (e.g. nickelhexahydrite; Gadd, Peter, Fraser et al., this volume). A handheld X-ray fluorescence (XRF) instrument can be used to readily and rapidly differentiate between HEBS mineralization and unmineralized, bedded pyrite in the field. Although some metal (e.g. PGE and Au) contents are too low to be detected by this instrument, others in the diagnostic enrichment suite (e.g. Ni, Zn, Cu, Mo, Se, U, and V) are present in abundances that are amenable to detection. Limited airborne geophysical surveys (i.e. versatile time-domain electromagnetic and magnetic surveys) suggest that it is possible to broadly delineate the favourable stratigraphic contact but they have insufficient spatial resolution to recognize subtle variations within the HEBS mineralization (Dumala, 2007d). Focused soil, float, and stream-sediment geochemistry have proven to be the most reliable exploration tools in searching for HEBS (Parry and Carne, 1989; Caulfield, 1997; Dumala, 2007a, b, c, d; Gregory, 2008a, b, c, d).

Hyper-enriched black shale mineralization may occur in several discrete layers (e.g. at the Peel River showing; Gadd and Peter, 2018; Gadd et al., 2019b) that are stratigraphically close enough to each other that they would constitute a single mining interval, or it may occur in a single, thicker-than-normal layer (up to approximately 2 m, Moss showing; Dumala, 2007d); such features may further enhance their economic potential. Another strategy to identify potentially economic targets might be to explore for structurally thickened mineralization (e.g. fold hinges, isoclinal and recumbent folds, and/or thrust stacking). Finally, it may be possible (and profitable) to mine lower grade material and process it using biohydrometallurgy to recover metals, rather than conventional methods (e.g. crushing, milling, and producing one or more concentrates). Such an approach is being applied at the Terrafame (formerly Talvivaara) Ni-Zn-Cu-Co open-pit mine, Finland (Riekkola-Vanhanen, 2007, 2010), in a climate similar to that of the northern Canadian Cordillera.

KNOWLEDGE GAPS AND FUTURE RESEARCH

Future studies should aim to gain a better understanding of shale sedimentology, particularly because the Selwyn Basin and the Richardson trough are geographically extensive with long shale depositional histories. Along the same lines, more stratigraphic sections of upper Silurian to Upper Devonian basinal strata should be measured because the most prospective strata — Middle Devonian black shale at the stratigraphic contact between the Road River Group and Canol Formation — may be readily identified in such field excursions. Prospective strata may strike for greater than 1000 km, providing ample opportunity to identify the HEBS in broader settings.

Tighter age constraints, either through refined radiometric geochronology or more detailed biostratigraphy, may significantly aid in the understanding of HEBS-forming mechanisms. Currently, a broad Middle Devonian age determination precludes a better understanding of which (if any) biotic crisis controlled HEBS formation. Existing samples may yield new results if conodont extraction techniques are developed for indurated shale-hosted semi-massive sulfides.

Future studies may also investigate secular changes in other nontraditional isotopic systems. Stable Se, Hg, Pt, or U isotopes seem like strong candidates because these systems are used to assess metallic sources and redox processes in earth surface environments. Such data would ideally complement existing isotopic studies but may also expand to geographic areas that have not been studied with these techniques.

CONCLUSIONS

Hyper-enriched black shale mineralization is geographically widespread in Middle Devonian strata in northern Yukon and northeastern British Columbia. Elements likely sourced from ambient seawater were Ni, Fe, Mo, Zn, Pt, Pd, Re, Au, and S. They were likely sequestered and deposited by Fe-Mn–oxyhydroxide particulate shuttling and during sulfidic diagenesis. The sulfur was derived from seawater sulfate, which was reduced by the interaction of microbes and organic matter via the process of bacterial sulfate reduction. The resultant sulfide mineralogy is dominated by pyrite, millerite or vaesite, and sphalerite and the sulfide mineral textures strongly support mineralization that initiated during earliest diagenesis and persisted into later diagenesis. The rare occurrence of late sulfide veins indicates that sulfide precipitation likely ceased during diagenesis; this is supported by tightly constrained radiometric ages at the Nick (390.7 ± 5.1 Ma), Peel River (387.3 ± 4.4 Ma), and Moss (389.4 ± 5.7 Ma) localities. There is close agreement between conodont biostratigraphic and radiometric ages, providing strong support that HEBS mineralization was a coeval, synsedimentary, basin-scale phenomenon.

The confluence of several environmental factors was essential to HEBS formation and preservation. Partially oxygenated marine redox conditions allowed for Fe-Mn oxyhydroxides to precipitate and accumulate metals and shuttle the metals to the seafloor. Exceptional primary productivity generated large amounts of organic carbon that was also exported to the seafloor. Both types of chemical sediments likely accumulated and concentrated hydrogenous metals. Favourable physical conditions include a trough setting that was amenable to periodically restricted connectivity with open marine conditions. Formation of HEBS coincides with periods of eustatic sea-level rise; therefore, it is likely that high sea levels starved the basin of clastic sediments, which ultimately allowed the HEBS to precipitate without dilution and preserved the metal tenors that are currently present.

Given the occurrence of HEBS at the regional exposure of the stratigraphic contact between the Road River Group and the Canol Formation, together with the recessive weathering of the host strata, exploration for HEBS mineralization should be focused on bedrock exposures in high-relief areas such as stream and river cuts, and cliff faces. That HEBS are coeval at localities separated by hundreds to thousands of kilometres indicates a strong potential for further discoveries elsewhere along the known stratigraphic contact between the Road River Group and the Canol Formation.

ACKNOWLEDGMENTS

This report is a contribution to NRCan's Targeted Geoscience Initiative (TGI) program. Support for this study was provided through the Volcanic- and Sedimentary-hosted Base Metal Mineralization project's Activity VS-1.2: Development of genetic and exploration models for hyper-enriched black shale (HEBS) deposits. Additional funding and field logistical support came from the Polar Continental Shelf program (Projects 007-17 and 010-18). We thank Tiffani Fraser and Leyla Weston of the Yukon Geological Survey for sharing their knowledge of Yukon shales with us; Nick Johnson of ZincX Resources for providing access to drill core and hosting us in the Akie exploration camp; and Claire Leighton, Isobel Crawford, and Krebchov Haimbodi of Queen's University for their assistance in the field. Simon Jackson, Zhaoping Yang, and Duane Petts (Geological Survey of Canada) provided critical assistance with LA-ICP-MS. We gratefully acknowledge Wayne Goodfellow and Larry Hulbert for providing access to legacy sample and data collections.

REFERENCES

Algeo, T.J. and Tribovillard, N., 2009. Environmental analysis of paleoceanographic systems based on molybdenum–uranium covariation; Chemical Geology, v. 268, no. 3–4, p. 211–225. https://doi.org/10.1016/j.chemgeo.2009.09.001

Becker, R.T., Gradstein, F.M., and Hammer, O., 2012. The Devonian period; Chapter 22 *in* The geological time scale 2012, (ed.) F.M. Gradstein, J.G. Ogg, M. Schmitz, and G. Ogg; Elsevier, p. 559–601. https://doi.org/10.1016/C2011-1-08249-8

Brett, C.E., Zambito, J.J., McLaughlin, P.I., and Emsbo, P., 2018. Revised perspectives on Devonian biozonation and environmental volatility in the wake of recent time-scale revisions; Palaeogeography, Palaeoclimatology, Palaeoecology, corrected proof. https://doi.org/10.1016/j.palaeo.2018.06.037

Caulfield, D., 1997. 1996 exploration program on the Rein property Prepared for Blackstone Resources Inc.; Energy, Mines and Resources, Yukon Geological Survey, Assessment Report 093594, 148 p. <http://yma.gov.yk.ca/093594.pdf> [accessed November 23, 2016]

Cecile, M.P., Morrow, D.W., and Williams, G.K., 1997. Early Paleozoic (Cambrian to Early Devonian) tectonic framework, Canadian Cordillera; Bulletin of Canadian Petroleum Geology, v. 45, no. 1, p. 54–74. https://doi.org/10.35767/gscpgbull.45.1.054

Cheng, M., Li, C., Zhou, L., Algeo, T.J., Zhang, F., Romaniello, S., Jin, C.-S., Lei, L.-D., Feng, L.-J., and Jiang, S.-Y., 2016. Marine Mo biogeochemistry in the context of dynamically euxinic mid-depth waters: a case study of the lower Cambrian Niutitang shales, South China; Geochimica et Cosmochimica Acta, v. 183, p. 79–93. https://doi.org/10.1016/j.gca.2016.03.035

Cohen, A., 2004. The rhenium–osmium isotope system: applications to geochronological and palaeoenvironmental problems; Journal of the Geological Society, v. 161, no. 4, p. 729–734. https://doi.org/10.1144/0016-764903-084

Coveney, R.M., Jr., Murowchick, J.B., Grauch, R.I., Glascock, M.D., and Denison, J.R., 1992. Gold and platinum in shales with evidence against extraterrestrial sources of metals; Chemical Geology, v. 99, no. 1-3, p. 101–114. https://doi.org/10.1016/0009-2541(92)90033-2

Crawford, I., Layton-Matthews, D., Peter, J.M., Gadd, M.G., and Voinot, A., 2019. Toward the application of molybdenum and thallium isotopes as indicators of paleoredox conditions and genesis of hyper-enriched black shale (HEBS) deposits, Peel River, Yukon; *in* Targeted Geoscience Initiative: 2018 report of activities, (ed.) N. Rogers; Geological Survey of Canada, Open File 8549, p. 139–161. https://doi.org/10.4095/313647

Dellwig, O., Leipe, T., März, C., Glockzin, M., Pollehne, F., Schnetger, B., Yakushev, E.V., Böttcher, M.E., and Brumsack, H.-J., 2010. A new particulate Mn–Fe–P-shuttle at the redoxcline of anoxic basins; Geochimica et Cosmochimica Acta, v. 74, no. 24, p. 7100–7115. https://doi.org/10.1016/j.gca.2010.09.017

Douville, E., Bienvenu, P., Charlou, J.L., Donval, J.P., Fouquet, Y., Appriou, P., and Gamo, T., 1999. Yttrium and rare earth elements in fluids from various deep-sea hydrothermal systems; Geochimica et Cosmochimica Acta, v. 63, no. 5, p. 627–643. https://doi.org/10.1016/S0016-7037(99)00024-1

Dumala, M., 2007a. Assessment report describing prospecting and geological mapping at the El property. Prepared for Southampton Ventures Inc. and Strategic Metals Ltd.; Energy, Mines and Resources, Yukon Geological Survey, Assessment Report 094960, 279 p. <http://yma.gov.yk.ca/094960.pdf> [accessed November 16, 2016]

Dumala, M., 2007b. Assessment report describing prospecting and geological mapping at the Mon property. Prepared for Southampton Ventures Inc. and Strategic Metals Ltd.; Energy, Mines and Resources, Yukon Geological Survey, Assessment Report 094890, 37 p. <http://yma.gov.yk.ca/094890.pdf> [accessed November 16, 2016]

Dumala, M., 2007c. Assessment report describing prospecting and geological mapping at the Pe property. Prepared for Southampton Ventures Inc. and Strategic Metals Ltd.; Energy, Mines and Resources, Yukon Geological Survey, Assessment Report 094869, 151 p. <http://yma.gov.yk.ca/094869.pdf> [accessed November 16, 2016]

Dumala, M., 2007d. Assessment report describing prospecting, mapping, geochemical sampling, geophysical surveys and diamond drilling at the Rich property. Prepared for Southampton Ventures Inc. and Strategic Metals Ltd.; Energy, Mines and Resources, Yukon Geological Survey, Assessment Report 094891, 455 p. <https://yma.gov.yk.ca/094891/094891.pdf> [accessed November 16, 2016].

Ellwood, B.B., Benoist, S.L., El Hassani, A., Wheeler, C., and Crick, R.E., 2003. Impact ejecta layer from the mid-Devonian: possible connection to global mass extinctions; Science, v. 300, no. 5626, p. 1734–1737. https://doi.org/10.1126/science.1081544

Emsbo, P., Hofstra, A.H., Johnson, C.A., Koenig, A.E., Grauch, R. I., Zhang, K.C., Hu, R.Z., Su, W.C., and Pi, D.H., 2005. Lower Cambrian metallogenesis of South China: interplay between diverse basinal hydrothermal fluids and marine chemistry; *in* Mineral deposit research: meeting the global challenge, (ed.) J. Mao and F.P. Bierlein; Springer-Verlag, Berlin, Heidelberg, p. 115–118. https://doi.org/10.1007/3-540-27946-6_30

Fan, J., Shen, S., Erwin, D.H., Sadler, P.M., MacLeod, N., Cheng, Q., Hou, X., Yang, J., Wang, X., Wang, Y., Zhang, H., Chen, X., Li, G., Zhang, Y., Shi, Y., Yuan, D., Chen, Q., Zhang, L., Li, C., and Zhao, Y., 2020. A high-resolution summary of Cambrian to Early Triassic marine invertebrate biodiversity; Science, v. 367, no. 6475, p. 272–277. https://doi.org/10.1126/science.aax4953

Fraser, T.A. and Hutchison, M.P., 2017. Lithogeochemical characterization of the Middle–Upper Devonian Road River Group and Canol and Imperial formations on Trail River, east Richardson Mountains, Yukon: age constraints and a depositional model for fine-grained strata in the Lower Paleozoic Richardson trough; Canadian Journal of Earth Sciences, v. 54, no. 7, p. 731–765. https://doi.org/10.1139/cjes-2016-0216

Gadd, M.G. and Peter, J.M., 2018. Field observations, mineralogy and geochemistry of Middle Devonian Ni-Zn-Mo-PGE hyper-enriched black shale deposits, Yukon; *in* Targeted Geoscience Initiative: 2017 report of activities, volume 1, (ed.) N. Rogers; Geological Survey of Canada, Open File 8358, p. 193–206. https://doi.org/10.4095/306475

Gadd, M.G., Peter, J.M., Goodfellow, W., Jackson, S.E., and Yang, Z., 2017. Geology, geochemistry and mineralogy of hyper-enriched black shale deposits, Yukon *in* Proceedings of Exploration 17: sixth decennial international conference on mineral exploration, (ed.) V. Tschirhart and M.D. Thomas; Toronto, Canada, p. 841–845.

Gadd, M.G., Peter, J.M., Fraser, T.A., and Layton-Matthews, D., 2019a. Lithogeochemical and sulphur isotope indicators of environment of formation and genesis of the Moss hyper-enriched black shale showing, Yukon; *in* Targeted Geoscience Initiative: 2018 report of activities, (ed.) N. Rogers; Geological Survey of Canada, Open File 8549, p. 163–178. https://doi.org/10.4095/313648

Gadd, M.G., Peter, J.M., Jackson, S.E., Yang, Z., and Petts, D., 2019b. Platinum, Pd, Mo, Au and Re deportment in hyper-enriched black shale Ni-Zn-Mo-PGE mineralization, Peel River, Yukon, Canada; Ore Geology Reviews, v. 107, p. 600–614. https://doi.org/10.1016/j.oregeorev.2019.02.030

Gadd, M.G., Peter, J.M., Hnatyshin, D., Creaser, R., Gouwy, S.A., and Fraser, T.A., 2020. A Middle Devonian basin-scale precious metal enrichment event across northern Yukon (Canada); Geology, v. 48, no. 3, p. 242–246. https://doi.org/10.1130/G46874.1

Garrett, R.G., Goodfellow, W., and Lund, N.G., 1977. Uranium reconnaissance program national stream sediment + water geochemical reconnaissance data northern Yukon Territory; Geological Survey of Canada, Open File 418, 14 p. https://doi.org/10.4095/129222

Goodfellow, W.D., 1987. Anoxic stratified oceans as a source of mineral in sediment-hosted stratiform Zn-Pb deposits (Selwyn Basin, Yukon, Canada); Chemical Geology: Isotope Geoscience section, v. 65, no. 3-4, p. 359–382. https://doi.org/10.1016/0168-9622(87)90014-5

Goodfellow, W.D., 2007. Base metal metallogeny of the Selwyn Basin, Canada; *in* Mineral deposits of Canada: a synthesis of major deposit types, district metallogeny, the evolution of geological provinces, and exploration methods, (ed.) W.D. Goodfellow; Geological Association of Canada, Mineral Deposits Division, Special Publication No. 5, p. 553–579.

Goldhaber, M.B. and Kaplan, I.R., 1980. Mechanisms of sulfur incorporation and isotope fractionation during early diagenesis in sediments of the gulf of California; Marine Chemistry, v. 9, no. 2, p. 95–143. https://doi.org/10.1016/0304-4203(80)90063-8

Gregory, D., 2008a. Assessment report describing prospecting, mapping and geochemical sampling at the Harken Property. Prepared for Strategic Metals Ltd.; Energy, Mines and Resources, Yukon Geological Survey, Assessment Report 095040, 86 p. <http://yma.gov.yk.ca/095040.pdf> [accessed March 4, 2020]

Gregory, D., 2008b. Assessment report describing prospecting, mapping and geochemical sampling at the Harlot Property. Prepared for Strategic Metals Ltd.; Energy, Mines and Resources, Yukon Geological Survey, Assessment Report 095605, 77 p. <http://yma.gov.yk.ca/095605.pdf> [accessed March 4, 2020]

Gregory, D., 2008c. Assessment report describing prospecting, mapping and geochemical sampling at the Harlow Property. Prepared for Strategic Metals Ltd.; Energy, Mines and Resources, Yukon Geological Survey, Assessment Report 095610, 89 p. <http://yma.gov.yk.ca/095610.pdf> [accessed March 4, 2020]

Gregory, D., 2008d. Assessment report describing prospecting, mapping and geochemical sampling at the Harvest Property. Prepared for Strategic Metals Ltd.; Energy, Mines and Resources, Yukon Geological Survey, Assessment Report 095606, 76 p. <http://yma.gov.yk.ca/095606.pdf> [accessed March 4, 2020]

Haq, B.U. and Schutter, S.R., 2008. A chronology of Paleozoic sea-level changes; Science, v. 322, p. 64–68. https://doi.org/10.1126/science.1161648

Henderson, K.M., Williams-Jones, A.E., and Clark, J.R., 2019. Metal transport by liquid hydrocarbons: evidence from metalliferous shale and pyrobitumen, Yukon; *in* Targeted Geoscience Initiative: 2018 report of activities, (ed.) N. Rogers; Geological Survey of Canada, Open File 8549, p. 179–187. https://doi.org/10.4095/313650

Horan, M.F., Morgan, J.W., Grauch, R.I., Coveney, R.M., Jr., Murowchick, J.B., and Hulbert, L.J., 1994. Rhenium and osmium isotopes in black shales and Ni-Mo-PGE-rich sulphide layers, Yukon Territory, Canada, and Hunan and Guizhou provinces, China; Geochimica et Cosmochimica Acta, v. 58, no. 1, p. 257–265. https://doi.org/10.1016/0016-7037(94)90463-4

House, M.R., 1996. The Middle Devonian Kačák event; Proceedings of the Ussher Society, v. 9, p. 79–84.

House, M.R., 2002. Strength, timing, setting and cause of mid-Palaeozoic extinctions; Palaeogeography, Palaeoclimatology, Palaeoecology, v. 181, no. 1-3, p. 5–25. https://doi.org/10.1016/S0031-0182(01)00471-0

Hulbert, L.J., Gregoire, D., Paktunc, D., and Carne, R., 1992. Sedimentary nickel, zinc, and platinum-group-element mineralization in Devonian black shales at the Nick property, Yukon, Canada: a new deposit type; Exploration and Mining Geology, v. 1, no. 1, p. 39–62.

Johnson, S.C., Large, R.R., Coveney, R.M., Kelley, K.D., Slack, J.F., Steadman, J.A., Gregory, D.D., Sack, P.J., and Meffre, S., 2017. Secular distribution of highly metalliferous black shales corresponds with peaks in past atmosphere oxygenation; Mineralium Deposita, v. 52, p. 791–798. https://doi.org/10.1007/s00126-017-0735-7

Jørgensen, B.B., Isaksen, M.F., and Jannasch, H.W., 1992. Bacterial sulfate reduction above 100°C in deep-sea hydrothermal vent sediments; Science, v. 258, no. 5089, p. 1756–1757. https://doi.org/10.1126/science.258.5089.1756

Jowitt, S.M. and Keays, R.R., 2011. Shale-hosted Ni-(Cu-PGE) mineralisation: a global overview; Applied Earth Science; Transactions of the Institution of Mining and Metallurgy: Section B, v. 120, no. 4, p. 187–197. https://doi.org/10.1179/1743275812Z.00000000026

Kabanov, P., 2019. Devonian (c. 388–375 Ma) Horn River Group of Mackenzie Platform (NW Canada) is an open-shelf succession recording oceanic anoxic events; Journal of the Geological Society, v. 176, no. 1, p. 29–45. https://doi.org/10.1144/jgs2018-075

Kane, J. (ed.), 1993. The USGS reference sample Devonian Ohio Shale SDO-1, U.S. Geological Survey Bulletin 2046, 112 p.

Koschinsky, A. and Hein, J.R., 2017. Marine ferromanganese encrustations: archives of changing oceans; Elements, v. 13, no. 3, p. 177–182. https://doi.org/10.2113/gselements.13.3.177

Lane, L.S., 2007. Devonian–Carboniferous paleogeography and orogenesis, northern Yukon and adjacent Arctic Alaska; Canadian Journal of Earth Sciences, v. 44, no. 5, p. 679–694. https://doi.org/10.1139/e06-131

Lehmann, B., Nägler, T.F., Holland, H.D., Wille, M., Mao, J., Pan, J., Ma, D., and Dulski, P., 2007. Highly metalliferous carbonaceous shale and Early Cambrian seawater; Geology, v. 35, no. 5, p. 403–406. https://doi.org/10.1130/G23543A.1

Lehmann, B., Frei, R., Xu, L., and Mao, J., 2016. Early Cambrian black shale-hosted Mo-Ni and V mineralization on the rifted margin of the Yangtze Platform, China: reconnaissance chromium isotope data and a refined metallogenic model; Economic Geology, v. 111, no. 1, p. 89–103. https://doi.org/10.2113/econgeo.111.1.89

Loutit, T.S., Hardenbol, J., Vail, P.R., and Baum, G.R., 1988. Condensed sections: the key to age-dating and correlation of continental margin sequences; *in* Sea level changes: an integrated approach, (ed.) C.K. Wilgus, B.S. Hastings, H. Posamentier, J. Van Wagoner, C.A. Ross, and C.G.St.C. Kendall; SEPM Special Publication 42, p. 183–213. https://doi.org/10.2110/pec.88.01.0183

Machel, H.G., 2001. Bacterial and thermochemical sulphate reduction in diagenetic settings—old and new insights; Sedimentary Geology, v. 140, no. 1–2, p. 143–175. https://doi.org/10.1016/S0037-0738(00)00176-7

MacIntyre, D.G., 1998. Geology, geochemistry and mineral deposits of the Akie River area, northeast British Columbia; British Columbia Ministry of Energy and Mines, British Columbia Geological Survey, Bulletin 103, 91 p.

Mao, J., Lehmann, B., Du, A., Zhang, G., Ma, D., Wang, Y., Zeng, M., and Kerrich, R., 2002. Re-Os dating of polymetallic Ni-Mo-PGE-Au mineralization in Lower Cambrian black shales of South China and its geologic significance; Economic Geology, v. 97, no. 5, p. 1051–1061. https://doi.org/10.2113/gsecongeo.97.5.1051

McClay, K.R., Insley, M.W., and Anderton, R., 1989. Inversion of the Kechika trough, northeastern British Columbia, Canada; *in* Inversion tectonics, (ed.) M.A. Cooper and G.D. Williams; Geological Society, London, Special Publications, v. 44, p. 235–257. https://doi.org/10.1144/GSL.SP.1989.044.01.14

McGhee, G.R., Jr., Clapham, M.E., Sheehan, P.M., Bottjer, D.J., and Droser, M.L., 2013. A new ecological-severity ranking of major Phanerozoic biodiversity crises; Palaeogeography, Palaeoclimatology, Palaeoecology, v. 370, p. 260–270. https://doi.org/10.1016/j.palaeo.2012.12.019

Miller, C.A., 2004. Re-Os dating of algal laminites: reduction-enrichment of metals in the sedimentary environment and evidence for new geoporphyrins; M.Sc. thesis, University of Saskatchewan, Saskatoon, Saskatchewan, 143 p.

Morrow, D.W., 1999. Lower Paleozoic stratigraphy of northern Yukon Territory and northwestern District of Mackenzie; Geological Survey of Canada, Bulletin 538, 202 p. https://doi.org/10.4095/210998

Murray, R.W., 1994. Chemical criteria to identify the depositional environment of chert: general principles and applications; Sedimentary Geology, v. 90, no. 3-4, p. 213–232. https://doi.org/10.1016/0037-0738(94)90039-6

Murray, R.W., Buchholtz ten Brink, M.R., Jones, D.L., Gerlach, D.C., and Russ, G.P., III, 1990. Rare earth elements as indicators of different marine depositional environments in chert and shale; Geology, v. 18, no. 3, p. 268–271. https://doi.org/10.1130/0091-7613(1990)018%3C0268:REEAIO%3E2.3.CO;2

Narkiewicz, K., Narkiewicz, M., and Bultynck, P., 2016. Conodont biofacies of the Taghanic transgressive interval (middle Givetian): Polish record and global comparisons; *in* Devonian climate, sea level and evolutionary events, (ed.) R.T. Becker, P. Königshof, and C.E. Brett; Geological Society of London, Special Publications, v. 423, p. 201–222. https://doi.org/10.1144/SP423.2

Nielsen, S.G., Goff, M., Hesselbo, S.P., Jenkyns, H.C., LaRowe, D.E., and Lee, C.A., 2011. Thallium isotopes in early diagenetic pyrite – a paleoredox proxy?; Geochimica et Cosmochimica Acta, v. 75, no. 21, p. 6690–6704. https://doi.org/10.1016/j.gca.2011.07.047

Norris, A.W., 1997. Devonian; *in* Geology and mineral and hydrocarbon potential of northern Yukon Territory and Northwestern District of Mackenzie, (ed.) D.K. Norris; Geological Survey of Canada, Bulletin 422, p. 163–200. https://doi.org/10.4095/208893

Nozaki, Y., 1997. A fresh look at element distribution in the north Pacific Ocean; American Geophysical Union, EOS Transactions, v. 78, no. 21, p. 221–223. https://doi.org/10.1029/97EO00148

Pagès, A., Barnes, S., Schmid, S., Coveney, R.M., Jr., Schwark, L., Liu, W., Grice, K., Fan, H., and Wen, H., 2018. Geochemical investigation of the lower Cambrian mineralised black shales of South China and the late Devonian Nick deposit, Canada; Ore Geology Reviews, v. 94, p. 396–413. https://doi.org/10.1016/j.oregeorev.2018.02.004

Parry, D. and Carne, R., 1989. Report on geological mapping, geochemical sampling and diamond drilling at the Nick Property, Yukon. Prepared for Inco Limited, NDU Resources, Pak-Man Resources Inc. and 2001 Resource Industries Ltd.; Energy, Mines and Resources, Yukon Geological Survey, Assessment Report 092832, 339 p. <http://yma.gov.yk.ca/092832.pdf> [accessed on November 15, 2016]

Peter, J.M., Bocking, N., Gadd, M.G., Layton-Matthews, D., and Johnson, N., 2018a, Textural and mineralogical characterization of a Ni-Zn-rich black shale occurrence at the Akie property, Kechika Trough, northern British Columbia, and comparison with examples from Yukon; *in* Targeted Geoscience Initiative: 2017 report of activities, volume 1, (ed.) N. Rogers; Geological Survey of Canada, Open File 8358, p. 207–216. https://doi.org/10.4095/306476

Peter, J.M., Gadd, M.G., Layton-Matthews, D., and Voinot, A., 2018b. Reconnaissance thallium isotope study of zinc-lead SEDEX mineralization and host rocks in the Howard's Pass district, Selwyn Basin, Yukon: potential application to paleoredox determinations and fingerprinting of mineralization; *in* Targeted Geoscience Initiative: 2017 report of activities, volume 1, (ed.) N. Rogers; Geological Survey of Canada, Open File 8358, p. 173–191. https://doi.org/10.4095/306474

Piper, D.Z., and Calvert, S.E., 2009. A marine biogeochemical perspective on black shale deposition; Earth-Science Reviews, v. 95, p. 63–96.

Pugh, D.C., 1983. Pre-Mesozoic geology in the subsurface of Peel River map area, Yukon Territory and District of Mackenzie; Geological Survey of Canada, Memoir 401, 61 p. https://doi.org/10.4095/119498

Riekkola-Vanhanen, M., 2007. Talvivaara black schist bioheapleaching demonstration plant; Advanced Materials Research, v. 20–21, p. 30–33. https://doi.org/10.4028/www.scientific.net/AMR.20-21.30

Riekkola-Vanhanen, M., 2010. Talvivaara Sotkamo mine – bioleaching of a polymetallic nickel ore in subarctic climate; Nova Biotechnologica, v. 10, no. 1, p. 7–14.

Rudnick, R.L. and Gao, S., 2014. Composition of the continental crust; Chapter 1 *in* Volume 4: The crust; Treatise on geochemistry 2nd edition, (ed.) R.L. Rudnick; Elsevier, Oxford, UK, p. 1–51. https://doi.org/10.1016/B978-0-08-095975-7.00301-6

Schmitz, B., Ellwood, B.B., Peucker-Ehrenbrink, B., El Hassani, A., and Bultynck, P., 2006. Platinum group elements and $^{187}Os/^{188}Os$ in a purported impact ejecta layer near the Eifelian–Givetian stage boundary, Middle Devonian; Earth Science Reviews, v. 249, no. 3–4, p. 162–172. https://doi.org/10.1016/j.epsl.2006.07.024

Scholz, F., Siebert, C., Dale, A.W., and Frank, M., 2017. Intense molybdenum accumulation in sediments underneath a nitrogenous water column and implications for the reconstruction of paleo-redox conditions based on molybdenum isotopes; Geochimica et Cosmochimica Acta, v. 213, p. 400–417. https://doi.org/10.1016/j.gca.2017.06.048

Schutter, S.R., 1996. The Glenwood Shale as an example of a Middle Ordovician condensed section; *in* Paleozoic sequence stratigraphy: views from the North American Craton, (ed.) B.J. Witzke, G.A. Ludvigson, and J. Day; Geological Society of America Special Papers, v. 306, p. 55–65. https://doi.org/10.1130/0-8137-2306-X.55

Scott, C. and Lyons, T., 2012. Contrasting molybdenum cycling and isotopic properties in euxinic versus non-euxinic sediments and sedimentary rocks: refining the paleoproxies; Chemical Geology, v. 324–325, p. 19–27. https://doi.org/10.1016/j.chemgeo.2012.05.012

Shuster, A.M., Wallace, M.W., van Smeerdijk Hood, A., and Jiang, G., 2018. The Tonian Beck Spring Dolomite: marine dolomitization in a shallow, anoxic sea; Sedimentary Geology, v. 368, p. 83–104. https://doi.org/10.1016/j.sedgeo.2018.03.003

Sokolova, E.A., 2010. Influence of temperature on development of sulfate-reducing bacteria in the laboratory and field in winter; Contemporary Problems of Ecology, v. 3, p. 631–634. https://doi.org/10.1134/S1995425510060032

Stein, H., 2014. Dating and tracing the history of ore formation; Chapter 4 *in* Volume 13: Geochemistry of mineral deposits; Treatise on Geochemistry, 2nd Edition, (ed.) S.D. Scott; Elsevier, Oxford, UK, p. 87–118. https://doi.org/10.1016/B978-0-08-095975-7.01104-9

Steiner, M., Wallis, E., Erdtmann, B.-D., Zhao, Y., and Yang, R., 2001. Submarine-hydrothermal exhalative ore layers in black shales from South China and associated fossils — insights into a Lower Cambrian facies and bio-evolution; Palaeogeography, Palaeoclimatology, Palaeoecology, v. 169, no. 3–4, p. 165–191. https://doi.org/10.1016/S0031-0182(01)00208-5

Strauss, J.V., Fraser, T.A., Melchin, M.J., Allen, T.J., Malinowski, J., Feng, X., Taylor, J.F., Gill, B.C., and Sperling, E.A., 2020. The Road River Group of northern Yukon, Canada: Early Paleozoic deep-water sedimentation within the Great American Carbonate Bank; Canadian Journal of Earth Sciences. https://doi.org/10.1139/cjes-2020-0017

Sverjensky, D.A., 1984. Europium redox equilibria in aqueous-solution; Earth and Planetary Science Letters, v. 67, p. 70–78. https://doi.org/10.1016/0012-821X(84)90039-6

Tribovillard, N., Algeo, T.J., Lyons, T., and Riboulleau, A., 2006. Trace metals as paleoredox and paleoproductivity proxies: an update; Chemical Geology, v. 232,no. 1-2, p. 12–32. https://doi.org/10.1016/j.chemgeo.2006.02.012

Tribovillard, N., Algeo, T.J., Baudin, F., and Riboulleau, A., 2012. Analysis of marine environmental conditions based on molybdenum–uranium covariation—applications to Mesozoic paleoceanography; Chemical Geology, v. 324-325, p. 46–58. https://doi.org/10.1016/j.chemgeo.2011.09.009

Walliser, O.H., Bultynck, P., Weddige, K., Becker, R.T., and House, M.R., 1995. Definition of the Eifelian-Givetian stage boundary; Episodes, v. 18, no. 3, p. 107–114. https://doi.org/10.18814/epiiugs/1995/v18i3/002

Xu, L., Lehmann, B., Jingwen, M., Wenjun, Q., and Andao, D., 2011. Re-Os age of polymetallic Ni-Mo-PGE-Au mineralization in Early Cambrian black shales of south China—a reassessment; Economic Geology, v. 106, no. 3, p. 511–522. https://doi.org/10.2113/econgeo.106.3.511

Xu, L., Lehmann, B., and Mao, J., 2013. Seawater contribution to polymetallic Ni–Mo–PGE–Au mineralization in Early Cambrian black shales of South China: evidence from Mo isotope, PGE, trace element, and REE geochemistry; Ore Geology Reviews, v. 52, p. 66–84. https://doi.org/10.1016/j.oregeorev.2012.06.003

Yin, R., Xu, L., Lehmann, B., Lepak, R.F., Hurley, J.P., Mao, J., Feng, X., and Hu, R., 2017. Anomalous mercury enrichment in Early Cambrian black shales of South China: mercury isotopes indicate a seawater source; Chemical Geology, v. 467, p. 159–167. https://doi.org/10.1016/j.chemgeo.2017.08.010